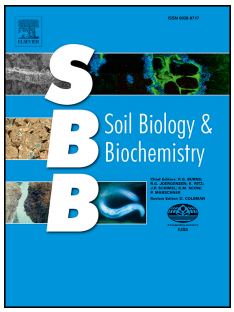

Life at the extreme: Plant-driven hotspots of soil nutrient cycling in the hyper-arid core of the Atacama Desert

Davey L. Jones, Bárbara Fuentes, Franko Arenas-Díaz, Francisco Remonsellez, Rutger van Hall, Brian S. Atkinson, Sacha J. Mooney, Roland Bol

PII: S0038-0717(23)00190-6

DOI: https://doi.org/10.1016/j.soilbio.2023.109128

Reference: SBB 109128

To appear in: *Soil Biology and Biochemistry*

Received Date: 6 June 2023

Revised Date: 10 July 2023

Accepted Date: 19 July 2023

Please cite this article as: Jones, D.L., Fuentes, Bá., Arenas-Díaz, F., Remonsellez, F., van Hall, R., Atkinson, B.S., Mooney, S.J., Bol, R., Life at the extreme: Plant-driven hotspots of soil nutrient cycling in the hyper-arid core of the Atacama Desert, *Soil Biology and Biochemistry* (2023), doi: https://doi.org/10.1016/j.soilbio.2023.109128.

Life at the extreme: Plant-driven hotspots of soil nutrient cycling in the hyper-arid core of the Atacama Desert

Davey L. Jones[a,b,*], Bárbara Fuentes[c], Franko Arenas-Díaz[d], Francisco Remonsellez[e], Rutger van Hall[f] , Brian S. Atkinson[g], Sacha J. Mooney[g], Roland Bol[h,a]

[a] *SoilsWales, School of Natural Sciences, Bangor University, Gwynedd, LL57 2UW, UK*

[b] *SoilsWest, Centre for Sustainable Farming Systems, Food Futures Institute, Murdoch University, Murdoch, WA 6150, Australia*

[c] *Departamento de Ingeniería Química, Universidad Católica del Norte, Antofagasta, Chile*

[d] *Programa de Doctorado en Ciencias mención Geología, Departamento de Cs. Geológicas, Universidad Católica del Norte, Antofagasta, Chile*

[e] *Centro de Investigación Tecnológica del Agua en el Desierto-CEITSAZA, Universidad Católica del Norte, Antofagasta, Chile*

[f] *Institute for Biodiversity and Ecosystem Dynamics, University of Amsterdam, Science Park 904, 1090 GE, Amsterdam, The Netherlands*

[g] *Agricultural and Environmental Sciences, School of Biosciences, University of Nottingham, Nottingham, LE12 5RD, UK*

[h] *Institute of Bio- and Geosciences, Agrosphere Institute (IBG-3), Forschungszentrum Jülich, 52425 Jülich, Germany*

Corresponding author: Davey L. Jones

Corresponding author address: SoilsWales, School of Natural Sciences, Bangor University, Bangor, Gwynedd, LL57 2UW, UK

Corresponding author Tel: +44 1248 382579

Corresponding author E-mail: d.jones@bangor.ac.uk

ABSTRACT

The hyperarid core of the Atacama Desert represents one of the most intense environments on Earth, often being used as an analog for Mars regolith. The area is characterized by extremes in climate (e.g., temperature, humidity, UV irradiation) and edaphic factors (e.g., hyper-salinity, high pH, compaction, high perchlorates, and low moisture, phosphorus and organic matter). However, the halophytic C_4 plant *Distichlis spicata* appears to be one of the few species on the planet that can thrive in this environment. Within this habitat it captures windblown sand leading to the formation of unique structures and the generation of above-ground phyllosphere soil. Using a combination of approaches (e.g., X-ray Computed Tomography, TXRF, $\delta^{13}C/\delta^{15}N$ isotope profiling, microbial PLFAs, ^{14}C turnover, phosphate sorption isotherms) we examined the factors regulating the biogeochemical cycling of nitrogen (N), phosphorus (P) and carbon (C) in both vegetated and unvegetated areas. Our results showed that *D. spicata* rhizomes with large aerenchyma were able to break through the highly cemented topsoil layer leading to root proliferation in the underlying soil. The presence of roots increased soil water content, P availability and induced a change in microbial community structure and promoted microbial growth and activity. In contrast, soil in the phyllosphere exhibited almost no biological activity. Organic C stocks and recent C_4 plant derived input increased as follows: phyllosphere (1941 g C m^{-2}; 85% recent) > soils under plants (575 – 748 g C m^{-2}; 55-60%) > bare soils (491 – 642 g C m^{-2}; 9-17%). Due to the high levels of nitrate in soil (>2 t ha^{-1}) and high rates of P sorption/precipitation, our data suggest that the microbial activity is both C and P, but not N limited. Root-mediated salt uptake combined with foliar excretion and dispersal of NaCl into the surrounding area indicated that *D. spicata* was responsible for actively removing ca. 55% of the salt from the rhizosphere. We also demonstrate that NH_3 emissions may represent a major N loss pathway from these soil ecosystems during the processing of organic N. We attribute this to NH_3 volatilization to the high pH of the soil and slow rates of nitrification. In conclusion, we demonstrate that the

extremophile *D. spicata* physically, chemically and biologically reengineers the soil to create a highly bioactive hotspot within the climate-extreme of the Atacama Desert.

Keywords: Astrobiology, Biological hotspot, Nutrient cycling, Desert microbiology, Moisture availability, Yungay region.

1. Introduction

Hyper-arid environments are defined by an extremely low rainfall (annual precipitation of less than 60-100 mm), high evapotranspiration and an overall aridity index of <0.05 (UNEP 1997). Hyper-aridity not only severely limits the development of vegetation but also leads to soils that are significantly affected by salts (e.g. NaCl, KNO_3, $NaClO_4$; Wang et al., 2017). As salt accumulates in the superficial horizons due to high evapotranspiration and lack of precipitation, no leaching to deeper layers of the soil occurs leading to highly stratified soil profiles (Fuentes et al., 2022a). Despite the inhospitable conditions prevailing in hyper-arid environments, life exists, indicative that the biogeochemical recycling of key nutrients (C, N and P) can take place (Knief et al., 2020; Fuentes et al., 2022b). However, biogeochemical cycling is extremely heterogenous, being concentrated in discrete spatial and temporal hotspots of activity. For example, Ewing et al. (2008) showed that in arid and hyper-arid soils, rapid cycling of C occurs in spatially segregated patches at the soil surface with plants exerting strong control on the supply of organic C. In addition, several studies have reported plants and associated microbial communities in hyper-arid environments both participate in soil nutrient cycling and in the rapid turnover of carbon (C) and nitrogen (N), particularly in response to ephemeral inputs of moisture (Jones et al., 2018; Santander et al., 2021; Wu et al., 2021).

The hyper-arid zone of the Atacama Desert is widely studied due its unique aridity and the presence of microbial and plant extremophiles (Uritskiy et al., 2019; Morales-Tapia et al., 2021). Among its other attributes, its soil properties are often used as a proxy for the exploration of Mars and the search for life on other planets (Ewing et al., 2006; Azúa-Bustos et al., 2012;

Fletcher et al., 2012). Within the hyper-arid core of the Atacama Desert, the southern margin, known as Yungay, is frequently studied due to its extreme climate (Warren-Rhodes, 2006) with this region generally devoid of vegetation and considered absolute desert (Caceres et al., 2007). Within Yungay, however, very small patches of halophytic vegetation do exist on a desert alluvial fan within the Quebrada del Profeta which have become colonized by shrubs, predominantly *Distichlis spicata* (L.) Greene (Ingendesa, 1997). The plant and edaphic factors that enable *D. spicata* to survive in one of the most extreme environments on Earth, however, are lacking. Unlike many ecosystems, plants in the Atacama Desert are rarely N limited due to the presence of extensive potassium and sodium nitrate deposits at the soil surface (Sutter et al., 2007; Voigt et al., 2020).

Plants that survive in the Atacama desert contribute to the emergence of highly heterogeneous landscapes, along with generating fertility islands and biodiversity hotspots (Castillo et al., 2017). Such areas are typically characterized by soils with higher moisture and nutrient content, as well as, enhanced microbial activities compared with the surrounding bare soils (Garner and Steinberger, 1989; Kidron, 2009; Gao et al., 2022). The plants themselves provide niches for microbial communities to thrive including bacteria, fungi, protists, nematodes and viruses (Trivedi et al., 2020). These above-ground niches include the phyllosphere and leaf endosphere, while below ground they include the endo- and ecto-rhizosphere (Araya et al., 2020; Arndt et al., 2020). In the case of *D. spicata*, its above-ground stems and foliage also captures a large amount of wind-blown soil, leading to the formation of a unique plant structure and the formation of large amounts of phyllosphere soil suspended above the traditional soil surface. Although not yet demonstrated in the Atacama desert, other niches promoted by the presence of plants may include endolithic microbial communities and biocrusts due to the provision of shade, enhanced humidity and the buffering of climate extremes (She et al., 2022).

In hyper-arid regions, the above-ground habitat for microorganisms are directly influenced by plant metabolism, however, abiotic factors are thought to dominate colonization potential (e.g., temperature, relative humidity, solar radiation, dust input) (Compant et al., 2019; Liu et al., 2023). In comparison, microbial communities below-ground in hyper-arid soils are likely to be more shaped by biotic factors (i.e., plant litter inputs, root exudation, symbiotic associations) as well as abiotic factors (i.e., soil type, moisture, temperature pH, salinity, nutrient availability)(Alfaro et al., 2021).

Given the paucity of information on extremophile plant-soil interactions in hyper-arid ecosystems, the objective of this study was to (i) evaluate microbial activity and biogeochemical cycling in the presence and absence of *D. spicata* plants, (ii) compare the properties of topsoil and subsoils in comparison to soil accumulated above-ground in the phyllosphere.

2. Materials and methods

2.1. Site description

The study site was located within the Yungay area, in the hyper-arid core of the Atacama Desert at Oficina Yugoslavia, Antofagasta, Chile (24°3'28"S, 69°49'33"W; 948 m above sea level) (Figs. S1-S2). It receives < 2 mm rain per year and has a mean annual temperature of 14-16 °C with a maximum of 37.9 °C and minimum of -5.7 °C (Warren-Rhodes et al., 2006; McKay et al., 2003). The extremely infrequent rainfall events can leave free water in the surface soil for ca. 3 d while it takes 10 d for the soil water content to revert back to pre-rainfall conditions (McKay et al., 2003). The relative humidity of the air at the site can vary from 1 to 95% depending on the presence of atmospheric fogs (Cáceres et al., 2007; Azúa-Bustos et al., 2011). The site experiences some of the most extreme potential evapotranspiration rates (ca. 1-2 mm d^{-1}; Mintz and Walker 1993), surface UV radiation and total solar irradiances measured on Earth (Cordero et al., 2018; Rondanelli et al., 2015). Geomorphic studies suggest that the

field site has experienced a near-continuous hyperarid climate since the late Pliocene (3 Mya; Amundson et al., 2012).

The zone of study is in a low-lying position and experiences sporadic drainage from torrential but very infrequent rainfall events which has led to the creation of an alluvial fan composed of gravels and lenses of unconsolidated coarse sand (Ferrando et al., 2013; Pfeiffer et al., 2021). The site is located over a desert alluvial fan cut by the Quebrada del Profeta in which a series of dry stream beds have become colonized by higher plants, predominantly *D. spicata* (L.) Greene (Poaceae; common name: Grama salada or Desert saltgrass)(Figs. S3-S4). Away from the streambed, no plant colonization occurred suggesting that this was an ephemeral moisture hotspot within the landscape (Fig. S3). Although the site is located within the hyper-arid core of the Atacama Desert, we established that groundwater is located 6 m below the ground surface (at location 24°03'12"S, 69°49'18"W). Plants were present in two distinct growth forms: (i) plants low to the ground (mean shoot height 12 ± 3 cm, n = 20), or (ii) plants in dense upright columns (mean height 112 ± 6 cm, mean width 78 ± 8 cm; n = 5; Fig. S3). These columns consist of dense clumps of stems that facilitate the accretion of windblown dust (i.e., phyllosphere soil), however, some soil may also have been eroded from the base of the plants during past torrential rain events (Fig. S4). This study only focused on the column forms of *D. spicata*.

2.2. Sample collection

Individual similar-sized columns of *Distichlis spicata* (n = 5) were randomly selected within a 100 × 100 m study area. The columns were located in different braids of the dry stream bed system. In addition, adjacent areas at least 5 m distant from the columns but containing no plants were used as reference controls (n = 5; Fig. S5). At each sampling location, 10 green shoots (12.3 ± 0.8 cm long), 10 senescent brown shoots (11.1 ± 1.0 cm long), short sections of stem (ca. 5 cm in length; diameter 3.18 ± 0.14 mm, n = 10) and roots were recovered from each

plant column. Root samples composed a composite of rhizomes (diameter 2.45 ± 0.26 mm, *n* = 10), primary roots (diameter 0.54 ± 0.03 mm, *n* = 10) and secondary roots (diameter 0.28 ± 0.01 mm, *n* = 10) relative to their abundance in the field. In addition, samples of the Atacama endemic shrubs *Atriplex atacamensis* Phil. (Amaranthaceae) (*n* = 4), *Adesmia atacamensis* Phil. (Fabaceae) (*n* = 2) and the tree *Prosopis tamarugo* Phil. (Fabaceae) (*n* = 1) growing at the study site were collected as reference controls for isotopic end-member analysis and nutrient comparisons.

The soil at the site is classified as a hyperaridic Typic Haplosalid (Finstad et al., 2014). Soil samples were collected at depth of 5-20 cm and 20-40 cm below the soil surface (with and without and *D. spicata* present). Unlike the top 0-5 cm, soil in these layers was not cemented and showed an abundance of roots in the *D. spicata* samples. No roots were observed in the bare soil controls. Additionally, soil samples of phyllosphere soil were taken from inside each of the *D. spicata* plant columns at a height of ca. 70 cm above the soil surface (Figs. S4-S6; Table S1). Intact soil samples containing roots were also collected from the cemented layer (ca. 0-5 cm) at base of the *D. spicata* plants. This sampling regime is shown schematically in Figs. S6-S7.

2.3. Soil and canopy temperature and humidity

To monitor diurnal patterns in soil temperature and relative humidity (RH), DS1923-F5 Hygrochron temperature and humidity data loggers (iButtonLink LLC, Whitewater, WI) were placed in the soil at two depths (1 cm, 10 cm) and within the vegetation canopy (phyllosphere soil). Data was recorded hourly from October, 2018 to March 2019 (6 months). The accuracy of the thermal measurements is ±0.5 °C and the RH measurements ±3.5%.

2.4. Plant analysis

Root and stem diameters were determined by image analysis. Plant moisture content was determined by oven-drying (80 °C, 48 h) and then ground to a fine powder using a MM200 ball mill (Retsch GmbH, Haan, Germany). Subsequently, their elemental composition was determined using a non-destructive S2 Picofox TXRF spectrometer (Bruker Inc., Billerica, MA) using Ga as an internal standard and validated using a range of certified plant standards (WEPAL-QUASIMEME, Wageningen, The Netherlands). The C, N, $\delta^{13}C$ and $\delta^{15}N$ contents of the milled plant samples were determined using a Vario Isotope cube connected with a BioVision Element continuous flow Isotope Ratio Mass Spectrometer (Elementar GmbH, Langselbold, Germany). Total C and N content were determined by peak integration as well as calibration against elemental standards. At least two calibrated laboratory standards were used to ensure the quality of analyses and to scale normalize the raw values to the international isotopic reference VPDB (^{13}C) and AIR (^{15}N). The standards were run before, in between and after the samples. Within the instrument software they were evaluated and used to calibrate the instrument on each run, do linearity checks and correction (as per de Groot, 2004) and required drift corrections. Standards included: lithium carbonate (^{13}C), IAEA-NBS18, calcite (^{13}C), IAEA-600, caffeine (^{13}C), IAEA-CH6, sucrose (^{13}C), IAEA-N2, ammonium sulfate (^{15}N) or IAEA-USGS-25, ammonium sulfate (^{15}N). The general precision of replicate analyses is estimated to be better than 5% (rel.) for C and N content and <0.1‰ for $\delta^{13}C$ and $\delta^{15}N$ content.

2.5. Soil characterisation

Samples were shipped to the UK under the UK Department for Environment, Food & Rural Affair plant health import licence number 52025/198560-6 in plastic containers. Upon arrival, moisture content was determined gravimetrically by oven drying (105 °C, 48 h). The chemical characteristics of the soils was determined by firstly shaking (200 rev min^{-1}, 30 min) 10 g of field-moist soil with 25 ml of distilled water. The pH and electrical conductivity (EC) of the extracts was then determined using standard electrodes. The extracts were then

centrifuged (24,000 *g*, 5 min) and the supernatant recovered. These were subsequently used for the analysis of soluble salts (Na, K, Ca) using a Sherwood 410 flame photometer (SciMed Ltd, Stockport, UK), P using the molybdate blue colorimetric procedure of Murphy and Riley (1962), NO_3^- using the vanadate colorimetric procedure of Miranda et al. (2001), NH_4^+ using the salicylate-based colorimetric method of Mulvaney (1996), total phenolics using the Folin-Ciocalteu procedure of Swain and Hillis (1959), and dissolved organic C (DOC) and N (DON) using an Multi N/C 2100S analyzer (Analytik Jena GmbH, Jena, Germany). $CaCO_3$ content was determined with a FOGL Benchtop Soil Calcimeter (BD Inventions, Thessaloniki, Greece). P sorption isotherms were determined by shaking different concentrations of $K_2H^{33}PO_4$ (5 ml, 5 to 280 mg P l^{-1}, 2.6 kBq) with 1 g of field-moist soil at 200 rev min^{-1} for 24 h. The suspensions were then centrifuged (18,000 *g*, 5 min) and the equilibrium P concentration determined by liquid scintillation counting using Optiphase HiSafe 3 scintillation fluid and a Wallac 1404 scintillation counter with automated quench correction (PerkinElmer Inc., Waltham, MA). The P buffer power (B_p) was calculated according to Barber (1995; see Supp Info). Available P was determined using 2 methods: (i) Olsen P method (0.5 M $NaHCO_3$ pH 8.5, 1:5 w/v extract; FAO, 2021), and (ii) acetic acid method (0.5 M CH_3COOH pH 2.5, 1:5 w/v extract (McCray et al., 2012). The sand, clay and silt particle size distribution was determined through textural analysis using a Micromeritics particle size analyser.

Comparable to plant samples analysis, soils were ground to a fine powder using a MM200 ball mill and then decalcified using 4 M HCl by adding enough acid until the samples finished bubbling. To get rid of the excess acid and moisture, the samples were freeze dried after which each sample was homogenized before weighing in for the subsequent EA-IRMS analysis as described above for the plant samples.

The percentage of new (here C_4-derived) carbon in the soil (F) was calculated as:

$$F = ((\delta^{13}C_{soil} - \delta^{13}C_{C_3soil}) - (\delta^{13}C_{C_4soil}\ ^{13}C_{C_3soil})) \times 100$$

with $\delta^{13}C_{soil}$ = $\delta^{13}C$ value of the actual soil or phyllosphere sample, $^{13}C_{C_3soil}$ = the $\delta^{13}C$ value of C_3 soil endmember (set at -26 ‰) and $\delta^{13}C_{C_4soil}$ = $\delta^{13}C$ value of C_4 soil endmember (set at -12 ‰). For more details see Balesdent et al. (1987). Plants with C_3 photosynthesis have $\delta^{13}C$ values ranging from approximately −32 to −22‰ (mean ca. −27‰), while those with C_4 photosynthesis have values ranging from about −17 to −9‰ (mean ca. −13‰) (Boutton et al., 1998). Studies by Diefendorf et al. (2010) and Kohn (2010) highlight that desert C_3 plants are expected to have $\delta^{13}C$ values above the global mean.

2.6 *X-ray Computed Tomography (CT)*

Samples were extracted from the soil as intact blocks of soil using a spade and placed in plastic boxes with packaging material to preserve the soil structure. These were then transported to the UK in Representative specimens of intact soil from the hard cemented soil surface layer (0-5 cm) were scanned on a Phoenix V|tome|X M 240 high resolution X-ray CT system (Waygate Technologies, Wunstorf, Germany) at the Hounsfield Facility, University of Nottingham, UK. The scanning parameters were optimized to allow balance between a large field of view and a high resolution. Each sample was imaged using a voltage and current of 170 kV and 160 µA respectively at a voxel size resolution of 58 µm. The specimen stage was rotated through 360° at a step increment of 0.143° over 36 minutes thus a total of 2520 projection images were obtained by averaging 3 frames (with 1 skip) with an exposure of 200 ms each, at every rotation step. Each scan was then reconstructed using DatosRec software (Waygate Technologies, Wunstorf, Germany). Radiographs were visually assessed for sample movement before being reconstructed in 16-bit depth volumes with a beam hardening correction of 6. Reconstructed volumes were then submitted for visualization in VG Studio MAX (version 2.2.0; Volume Graphics GmbH, Heidelberg, Germany).

Images of the soil specimens was undertaken using Image J (FiJI 64-bit). An assessment of each sample was undertaken by first creating a region of interest (ROI) for comparison between samples. Within each region, the separate segmentation of plant material was undertaken to ensure accurate characterization of soil morphological properties which was performed by creating a 'mask' in VG Studio MAX of the plant material i.e., roots/stems contained within the region of interest. This segmentation process was undertaken via manual application of a region growing algorithm. Once the ROI was created the Otsu algorithm in Image J was used to binarize the sample (i.e., discriminate the solid and pore space). The sample was then assessed as the entire sample/volume referred to as the bulk soil based on the largest rectangular region that fit within the irregular shaped sample. The samples were then separated visually into low density soil (i.e., high porosity) and high-density soil (i.e. low porosity) regions (considerably smaller than the bulk soil region, for further analysis). The separate regions were then assessed for the following morphological properties; porosity, pore size, pore size distribution and coefficient of uniformity (a ratio of the pore size distribution expressed by d_{60}:d_{10}).

2.7. Microbial activity and C use efficiency

To evaluate soil microbial activity, field-moist soil (5 g) from each site (topsoil, subsoil, phyllosphere soil) was placed in individual sterile 50 cm^3 polypropylene tubes. ^{14}C-glucose was then added to each sample (100 µl, 3.86 kBq) at either a low (10 µM; 14 ng C g^{-1}) or high rate (10 mM; 14 µg C g^{-1}) of C relative to the size of the microbial biomass. To capture the $^{14}CO_2$ released, a NaOH trap (1 ml) was suspended above the soil and the tubes hermetically sealed and incubated at 20 °C. The NaOH trap was replaced periodically over 48 d. The $NaH^{14}CO_3$ in the NaOH traps was determined by liquid scintillation counting as described above. At the end of the incubation period the soils were extracted with 1 M NaCl (1:5 w/v; 200 rev min^{-1}, 15 min), centrifuged (18,000 *g*, 10 min) and the amount of ^{14}C present in the

supernatant determined by liquid scintillation counting. NaCl was used in place of KCl to minimise the background associated with ^{40}K. Microbial C use efficiency (CUE) for the added substrates was calculated according to Jones et al. (2018), where

$$CUE = (^{14}C_{tot} - {}^{14}CO_2 - {}^{14}C_{NaCl})/(^{14}C_{tot} - {}^{14}C_{NaCl}) \quad \text{(Eqn. 1)}$$

and where $^{14}C_{tot}$ is the total amount of ^{14}C-glucose added to the soil, $^{14}CO_2$ is the amount of ^{14}C-glucose respired and $^{14}C_{NaCl}$ is the amount of ^{14}C recovered in the NaCl extract at the end of the experiment (i.e. unused substrate).

We also measured the microbial turnover of complex, plant-derived C across the different soil depths according to Glanville et al. (2012). Briefly, high molecular weight (MW) plant material was prepared by heating 2.5 g of ^{14}C-labeled *Lolium perenne* L. shoots (Hill et al., 2007) in distilled water (25 ml, 80 °C) for 2 h. The extract was then centrifuged (1118 *g*, 5 min) and the soluble fraction removed. The pellet was then re-suspended in distilled water and the heating and washing procedure repeated twice more until >95% of the water-soluble fraction had been removed. The pellet remaining was dried overnight at 80 ºC and ground to a fine powder. The heating ensured that the intrinsic microbial community in the plant material was minimized (Jones et al., 2018). The mineralization dynamics of the high MW plant material was determined by mixing 50 mg of ^{14}C-labelled plant material (42 kBq g^{-1}) with 5 g of field-moist soil. The production of $^{14}CO_2$ was monitored over 48 d as described above for ^{14}C-labelled glucose.

2.8. Soil microbial nitrogen dynamics

Potential net N mineralization was determined by anaerobic incubation according to Waring and Bremner (1964) and Kresoivć et al. (2005). Briefly, 2 g of field-moist soil was placed in 20 cm^3 polypropylene tubes and anaerobic conditions imposed by filling the tubes with distilled water and then sealing the tubes. Soil samples were then incubated for 10 d in the dark at 40ºC. Subsequently, the incubated samples were transferred to 50 cm^3 polypropylene

tunes and solid KCl was added to achieve a final concentration of 1 M KCl. The samples were then extracted by shaking for 30 min (200 rev min^{-1}), centrifuged (18000 *g*, 10 min) and NH_4^+ in the supernatant determined colorimetrically as described previously. Net ammonification was calculated as the amount of NH_4^+ present after 7 d minus that present at the start of the incubation.

To determine the rate of arginine mineralization, 0.2 ml of a ^{14}C-labelled L-arginine solution (50 mM; C:N ratio 6:4; 2.17 kBq ml^{-1}; 10 µmol g^{-1}; 0.56 mg N g^{-1}; Amersham Biosciences UK Ltd, Chalfont St Giles, Bucks, UK) was added to 1 g of field-moist soil in a sterile 50 cm^3 polypropylene tube (Kemmitt et al., 2006). A 1 M NaOH trap was suspended above the soil to catch any $^{14}CO_2$ evolved and the traps periodically changed over a 96 h as described above. In addition, a 2.1 cm diameter Whatman GF/C glass fibre filter paper (GE Healthcare Bio-Sciences, Pittsburgh, PA) impregnated with 0.15 M H_3PO_4 was suspended above the soil to capture any NH_3 emitted from the soil (Jones et al., 2012). At the end of the incubation period the NaOH and H_3PO_4 traps were removed. Subsequently, the NH_4^+ produced derived from the mineralization of arginine was determined by extracting the soil with 1 M KCl (1:5 w/v) as described previously. The H_3PO_4 impregnated filter papers in the NH_3 traps were vortexed with 0.9 ml of distilled water, centrifuged (18,000 *g*, 10 min) and their NH_4^+ content determined colorimetrically as above.

2.9. Microbial community structure

Microbial community structure was measured by phospholipid fatty acid (PLFA) analysis following the method of Buyer and Sasser (2012). Briefly, samples (2 g) were freeze-dried and Bligh-Dyer extractant (4.0 ml) containing an internal standard added. Tubes were sonicated in an ultrasonic bath for 10 min at room temperature before rotating end-over-end for 2 h. After centrifuging (10 min) the liquid phase was transferred to clean 13 mm × 100 mm screw-cap test tubes and 1.0 ml each of chloroform and water added. The upper phase was

334 removed by aspiration and discarded while the lower phase, containing the extracted lipids,
335 was evaporated at 30°C. Lipid classes were separated by solid phase extraction (SPE) using a
336 96-well SPE plate containing 50 mg of silica per well (Phenomenex, Torrance, CA).
337 Phospholipids were eluted with 0.5 ml of 5:5:1 methanol:chloroform:H_2O (Findlay, 2004) into
338 glass vials, the solution evaporated (70°C, 30 min). Transesterification reagent (0.2 ml) was
339 added to each vial, the vials sealed and incubated (37°C, 15 min). Acetic acid (0.075 M) and
340 chloroform (0.4 ml each) were added. The chloroform was evaporated just to dryness and the
341 samples dissolved in hexane. The samples were analyzed with a 6890 gas chromatograph
342 (Agilent Technologies, Wilmington, DE) equipped with autosampler, split-splitless inlet, and
343 flame ionization detector. Fatty acid methyl esters were separated on an Agilent Ultra 2
344 column, 25 m long × 0.2 mm internal diameter × 0.33 μm film thickness. Standard
345 nomenclature was followed for fatty acids (Frostegård et al., 1993) with affiliation of individual
346 fatty acids to taxonomic groups undertaken as described in Table S3.
347
348 *2.10. Statistical analysis*
349 Differences in major plant and soil characteristics were determined by a One-way or
350 two-way ANOVA, as appropriate, using Minitab v18.0 (Minitab Inc., State College, PA). $P <$
351 0.05 was used as the cut-off for statistical significance. Differences in soil microbial
352 community structure were evaluated with principal component analysis in Minitab v18.0.
353 Linear regression was used to evaluate relationships between variables in Minitab v18.0.
354 Values in the text represent means ± SEM unless otherwise stated.
355
356 **3. Results**
357 *3.1. Temperature and relative humidity of the plant canopy and the soil*
358 As expected, distinct diurnal patterns were apparent in the climate data (Fig. 1). Overall,
359 daytime mean temperatures values were similar over the 6-month period being 21.6°C in the

plant canopy, 25.1°C in the surface soil and 24.8°C in the subsurface soil. The mean daily oscillation in temperature, however, was largest in the surface soil (26.8°C), followed by the plant canopy (21.7°C), with much less temperature variation seen in the subsurface soil (10.9°C). The highest average temperatures in the plant canopy, surface soil and subsurface soil were recorded between 13:00 and 15:00 h and reached 36.6°C, 45.0°C and 36.1°C, respectively (Fig. 1A). The minimum temperatures were seen between 05:00-06:00 h reaching a low of 3.6°C, 6.5°C, and 11.1°C in the plant canopy, surface soil and subsurface soil, respectively (Table S2, Fig. S9).

The relative humidity (RH) was relatively constant in the soil and was always higher in the subsurface soil, with average values in the range of 47 and 49%; while lower values in the range of 21-29% were found in the surface soil (Fig. 1). The RH in the plant canopy reached its highest values at night until 06:00 h with values around 50%, then decreased sharply during daylight hours. The mean daily oscillation in RH was largest in the plant canopy (39.2%), while the daily variation in the surface and subsurface soil was much lower being 8.1% and 2.0%, respectively. The minimum and maximum RH recorded in the plant canopy was 3.6% and 77.7%, respectively (Table S2, Fig. S9).

3.2. Plant analyses

The macro- and micronutrient content of the different plant parts of *D. spicata* were significantly different for all analyzed elements, except S (fresh leaves, senescent leaves, stems and roots; Table 1). Analysis also confirmed that the fresh leaves contained high levels of NaCl with an abundance of salt crystals on the leaf surface (Fig. S10), with the highest levels seen in the photosynthetic leaves. The C/N ratio of the *D. spicata* leaves was higher than of the leaves of the other 3 species. The $\delta^{15}N$ content of *D. spicata* plant parts (12.0-21.7 ‰) was higher than leaves of the other 3 species (5.8-11.9 ‰) (Table 1; Figs. S10-11). Above and below ground plant ^{13}C values reflected their C_3, *Adesmia atacamensis* (-25.2 ‰) and *Prosopis tamarugo* (-

386 23.5 ‰) or C_4 photosynthetic pathway, *D. spicata* and (-13.2 to -15.3 ‰) and *Atriplex*
387 *atacamensis* (-15.0 ‰) (Table 1; Fig. S10).
388
389 *3.3. Soil analysis*
390 *3.3.1. Soil elemental and nutrient content*
391 There was no significant difference in soil textural properties (i.e. clay, silt or sand
392 content), in areas with and without *D. spicata* plants (Table 2). However, there were significant
393 differences for most of the other measured parameters, excepting NO_3^-, between the two
394 sampled areas (with plants and without plants) in the desert oasis (Table 2). The most
395 significant difference generally occurred between phyllosphere and other soil locations (top or
396 subsoil, independent of being with or without plants) (Table 2) with amounts in the
397 phyllosphere generally being double to up to two hundred times (for total phenol content) of
398 the rest of soil. Analysis confirmed the high Na^+ and NO_3^- content of the soil, particularly the
399 soil trapped in the plant canopy (Fig. S9). Overall, the soils were very low in plant-available P
400 (Table 2). The Olsen-P values (mean 1.8 mg P kg^{-1}) were much lower than those recovered
401 with an acetic acid extract (mean 30.3 mg P kg^{-1}; $P < 0.001$). Further, the results showed that
402 acetic acid extractable P was much greater in the soil with plants in comparison to the
403 unvegetated areas.
404 P sorption isotherms revealed that the soils under *D. spicata* and in the corresponding
405 unvegetated areas had an extremely high capacity to bind P (Fig. S17). In contrast, the
406 phyllosphere soil had a much lower capacity to bind P. This is exemplified in the average P
407 buffer power (B_p) in the aerial phyllosphere soil which was 11.5 ± 1.7 while it was 519 ± 93 in
408 the soil under the plants. Rates of ammonification assessed using the anaerobic incubation
409 assay showed no difference between planted and unplanted soils, however, large rates of net
410 NH_4^+ production were seen in the phyllosphere soil (Table 2).
411

412 *3.3.2. Pore morphology results from X-ray CT*

413 X-ray CT imaging revealed that the highly cemented (0-5 cm) layer at the base of the
414 plant pedestal had significant amounts of plant rhizome material passing through it (Fig. 2).
415 The presence of the cemented layer under the plants strongly suggested that it has formed prior
416 to plant establishment. Whilst the plant material was consistently orientated in the same vertical
417 direction, there was a clear structural discontinuity with respect to soil pore space. The pore
418 space of the specimens as a whole were generally quite porous (c. 20%) with an average pore
419 size of around 1 mm^2 and a relatively homogeneous pore size distribution (Fig. S10). However,
420 when assessed as high- and low-density regions, clear differences were observed. At the
421 resolution used in this study (58 µm), the porosity in the high-density region (directly at the
422 soil surface) was <1% compared to 16% in the underlying low-density areas (Table S3). While
423 the average pore sizes for the different regions are similar (0.13 and 0.20 mm^2 respectively for
424 high- and low-density regions), clear differences in the pore size distribution (and coefficient
425 of uniformity, PSD_{cu}) did occur with many more of the smaller sized pores in the low-density
426 region (Fig. S10, Table S3). Root material was clearly visible in both low- and high-density
427 regions and showed large amounts of aerenchyma present within the tissue (Hansen et al.,
428 1976; See Supplementary Movie S1 and Movie S2).

429

430 *3.3.3. Origin and amounts of soil C and N stocks*

431 Soil trapped in the *D. spicata* phyllosphere contained ca. 5 times higher levels of organic
432 C than the underlying soil which were generally very low in C (0.17 ± 0.01 g kg^{-1}; Table 2).
433 This trend was also reflected in the levels of dissolved organic C and extractable phenolics
434 which were also much higher in the phyllosphere soil. Soils in areas with and without plants
435 contained comparable amounts of organic C in the top- and underlying subsoil (Table 3).
436 However, in the unvegetated area only 9-17% of the C was present as C_4-C and thus from
437 recent plant C inputs. In contrast, in the areas with *Distichlis spicata* plants the values were

438 much higher ranging from 57-60% (Table 3). On an area basis, most of the organic C present
439 in the planted soils was found in the phyllosphere (1941 ± 866 g C m^{-2}). It contained double
440 the amount of C, although being only half the depth (10 cm) of the other sampled soil
441 compartments (Fig. S7). Furthermore, in the phyllosphere soil the organic C stocks consisted
442 of >85% of more recent C_4-C plant derived inputs, with the remainder being non-recent C_3
443 (Table 3; Fig. S12).
444
445 *3.4. Soil microbial communities*
446 Overall, the size of the microbial biomass was 11-fold higher under the *D. spicata* plants
447 in comparison to areas where no plants were present (Table 4). All other microbial parameters
448 (i.e. Gram-negative and Gram-positive bacteria, fungi, putative arbuscular mycorrhizal fungi,
449 actinomycetes) were also up to twenty-five times higher in the vegetated area (Table 4). With
450 respect to soil depth, no differences were seen in either the size or structure of the microbial
451 community in either the planted or unplanted areas. Based on the fatty acid profile, Gram-
452 positive bacteria were present at much higher levels than Gram-negative bacteria (ca. 2-fold
453 higher; $P < 0.001$), while fungal-specific or putative arbuscular mycorrhizal fungal fatty acid
454 markers could only be detected under *D. spicata*. The soil trapped in the phyllosphere had a
455 much lower microbial biomass, being comparable to that present in the unplanted areas (Table
456 4). In contrast to the unplanted top- and subsoils, the phyllosphere soil had a higher abundance
457 of fungi (Table 4). While the fungal PLFA marker used here (18:2w6c) has previously been
458 shown to be a reliable marker of fungal biomass (Frostegard and Bååth, 1996; Olsson, 1999;
459 Kaiser et al., 2010), we cannot discount that some may also have originated from plant litter
460 (Willers et al., 2015; Napier et al., 2014). Further qPCR, metabarcoding and metagenomic
461 approaches should therefore be used to confirm this result.
462
463 *3.5. Soil microbial activity and carbon and nitrogen mineralization*

464 The microbial turnover of a low dose of glucose added to the soil (10 µM) is shown in
465 Figure 3. Overall, the rate of glucose turnover was very rapid in the soil under *D. spicata*
466 relative to that in the bare soil devoid of plants ($P < 0.001$). This is evidenced by the ca. 16-
467 fold difference in mineralization rate between the two treatments in the first 24 h after substrate
468 addition. In contrast to the soil trapped in the phyllosphere, the bare soil showed evidence of a
469 lag phase in $^{14}CO_2$ evolution which lasted for ca. 7 d after glucose addition. No significant
470 difference in the rate of $^{14}CO_2$ evolution was observed between the topsoil and subsoil under
471 plants ($P = 0.403$) with the same response also observed in the bare soil area ($P = 0.841$). In
472 contrast to the soil under the plants, the phyllosphere soil showed very little capacity to
473 mineralize ^{14}C-glucose and exhibited a significant lag phase in $^{14}CO_2$ evolution. At the end of
474 the 48-d incubation period, only small amounts of ^{14}C-glucose could be recovered from the
475 planted soil (2.1 ± 0.6%) or from the bare soil areas (8.5 ± 0.2%) with a NaCl extract, indicating
476 that a large proportion of the ^{14}C had been immobilized in the microbial biomass. Our estimates
477 suggest that the amount of glucose-C immobilized did not differ significantly in the below-
478 ground treatments (48.5% of the total; $P = 0.898$). In contrast, in the phyllosphere soil 80 ±
479 16% of the ^{14}C glucose remained in the soil after 48 d with only 12 ± 9% immobilized in the
480 biomass.

481 The microbial response to the higher dose of glucose (10 mM) yielded similar patterns
482 to that seen at the lower glucose dose, except that the proportionate rates of mineralization were
483 much lower, and the lag phases were much longer (Fig. 4). In the rhizosphere soil the total
484 amount of $^{14}CO_2$ evolved was greater at the high glucose dose (64 ± 6%) in comparison to the
485 low dose addition (48 ± 3%; $P < 0.001$) and consequently the amount immobilized in the
486 microbial biomass was lower (34 ± 6% versus 49 ± 3%, respectively; $P < 0.001$). This led to
487 significant differences in microbial C use efficiency (CUE) between the two glucose treatments
488 in the soil under plants (Fig. 5). In contrast, no differences in CUE were seen in the soil without

plants irrespective of soil depth or substrate concentration ($P > 0.05$). No CUE values are presented for the phyllosphere soil due to the large uncertainty associated with the data.

The mineralization of the ^{14}C-labelled plant litter is shown in Figure 6. Overall, almost no mineralization of the plant material occurred over the 48-d incubation period in the phyllosphere soil. In contrast, significant breakdown was observed in the soil underlying the plants and to a lesser extent in the bare soil. Ten days after applying the plant litter, its rate of mineralization was 62-fold faster in the soils under plants relative to that in the bare soil or phyllosphere ($P < 0.001$).

The turnover of ^{14}C-labelled arginine and the subsequent production of NH_4^+ and NH_3 is shown in Figure 7. Following a similar pattern to glucose, the greatest rate of turnover was seen in the soil underlying the plants relative to the other treatments ($P < 0.001$). The rate of N mineralization was closely coupled to the rate of C mineralization, being greater in the vegetated top- and sub-soil ($r^2 = 0.84$; $P = 0.012$; Fig. S15). Large amounts of NH_3 were emitted from the phyllosphere and bare soil areas, relative to the amount of NH_4^+ recovered at the end of the incubation period suggesting that most of the mineralized N was lost in a gaseous form (Fig. 7C). This contrasts with the rhizosphere soil where proportionally more of the arginine-derived N was retained as NH_4^+ relative to NH_3 ($P < 0.023$). Despite this, a significant relationship was apparent between the rate of arginine-C mineralization and NH_3 production ($r^2 = 0.86$; Fig. S16).

4. Discussion

4.1. Plant survival at the hyperarid climate extreme

Consistent with previous reports, we show that the hyperarid core of the Atacama Desert experiences large diurnal variations in air temperature and relative humidity (Azúa-Bustos et al., 2015). When combined with low amounts of rainfall, soil moisture, soil surface compaction, high salinity and nutrient imbalance it makes it a highly challenging environment

515 for plants to survive (Marquet et al., 1998). The dominant plant, *D. spicata*, has a water efficient
516 C_4 metabolism, is hyper-salt tolerant (i.e. survival at >0.5 M NaCl) and can withstand
517 temperatures of up to 57°C (Golden et al., 1995; Warren and Brockelman, 1989; Lazarus et al.,
518 2011). This halophytic trait is reflected in the high contents of NaCl in the leaves, the
519 abundance of salt crystals on the leaf surface (Fig. S6b) and the presence of high amounts of
520 salt in the phyllosphere soil. A comparison of salt in the vegetated and unvegetated soils
521 suggests that *D. spicata* is effective at removing salt from the soil and discharging it into the
522 above-ground component. For example, much lower levels of Na were seen in the roots relative
523 to the shoots and in the subsoil relative to the phyllosphere soil. Our observations are also
524 consistent with the excretion of Na via foliar salt glands in this plant (Semenova et al., 2010;
525 Hasanuzzaman et al., 2014). Similar to Morris et al. (2019) we observed salt crystals on the
526 leaf surface ranging in size from 25-100 μm in diameter. We speculate that these crystals will
527 be blown off the leaf surface into the surrounding area (via the process of haloconduction; Yun
528 et al., 2019), while other crystals become trapped within the phyllosphere soil. Based on the
529 reduction of Na in soil under the plants, we estimate that the plants have effectively removed
530 ca. 55% of the Na from the underlying soil, supporting the proposed use of halophytic salt
531 shedding plants for land remediation purposes (Litalien et al., 2020).

532 As evidenced by the X-ray CT scans, the soil at the field site has an extremely hard and
533 cemented surface horizon underlain by a more porous subsoil. We observed aerenchymous
534 rhizomes of *D. spicata* with sharp points passing through this layer. After passage through this
535 cemented layer there was a proliferation of secondary and tertiary roots. Our results are
536 consistent with Hansen et al. (1976) who observed an abundance of epidermal silica cells which
537 are thought to facilitate passage through highly compacted soil. These rhizomes are also likely
538 to facilitate clonal growth and lateral plant establishment observed at the field site (Brewer and
539 Bertness, 1996). The highly cemented layer is likely to restrict air movement into the soil
540 (Weiler, 2005). Although we did not test this directly, the presence of large amounts of

aerenchyma tissue in the vertical rhizomes passing through the cemented layer would support this (Colmer and Flowers, 2008).

4.2. Soil moisture in the hyperarid core of the Atacama Desert

We observed that soil moisture was higher in the vegetated areas in comparison to unvegetated areas, the latter being similar to those reported previously (Fuentes et al., 2022a). Although the origin of this water was not investigated, we speculate that *D. spicata*, which is known to be deep rooting, employs hydraulic lift to bring up groundwater and redistribute it into the upper soil layers to promote microbial activity, nutrient uptake and Na detoxification (Dawson, 1993; Armas et al., 2010). As the intrinsic moisture content in the phyllosphere soil was extremely low, we conclude that there is no evidence for hydraulic lift in this plant-soil compartment. Further work looking at the salinity and isotopic signature of the groundwater and constraints to water, however, are still needed (Bazihizina et al., 2017). The columnar structure growth form is uncommon for *D. spicata*, which typically grows low to the ground (Hansen et al., 1976). We speculate that columnar growth may confer some advantages for water conservation in the hyperarid core including: (i) provision of a windbreak, (ii) offering a large surface area for the condensation of fog water, (iii) lowering air and soil temperatures, all of which would decrease evaporation, positively affecting the soil moisture balance (Fuentes et al., 2022b; Sotomayor et al., 2019). This is supported by previous studies showing that other plants in the Atacama Desert actively manage their micro-environment and moderate soil conditions, particularly on the driest and hottest days (Sotomayor et al., 2019).

4.3. Size and structure of the microbial community in hyperarid soils

As expected, the size of the soil microbial community was greatly enhanced in the presence of plants leading to the creation of biological hotspots within the hyperarid core of the Atacama Desert. Due to the cemented layer preventing leaf litter entering the soil, we

ascribe this stimulation of microbial biomass and activity entirely due to rhizodeposition (root exudation and root/mycorrhizal turnover), the plant-mediated reduction in salt and the greater abundance of soil water (Jones et al., 2009). Evidence for the presence of arbuscular mycorrhizal fungi (AMF) is provided by the sole detection of the putative AMF PLFA marker 16:1w5c in the soil under the plants, and its absence from soil collected from the phyllosphere and unvegetated areas. It is also supported by previous reports describing the strong colonization of *D. spicata* by AMF in saline soils (Allen and Cunningham, 1983; Eppley et al., 2009). The origin, diversity of AMF spores and their functional role in promoting plant growth in these hyperarid soils requires further investigation (i.e. nutrient and water uptake, stress tolerance), however, we assume that they are involved in promoting P acquisition given the low amounts and poor availability of P in our soils (Fig. S17). Interestingly, the presence of AMF appears to be related to the dioecious nature of *D. spicata* with differences in root colonization between male and female plants and that this difference in AMF may be linked to greater water use efficiency (Eppley et al., 2009; Reuss-Schmidt et al., 2015). Whether this sex trait links to plant performance in hyperarid climates and differences in growth forms is unknown and warrants further study.

In contrast to soils with no moisture limitation, all our samples showed a greater Gram-positive-to-Gram-negative ratio reflecting the adverse edaphic conditions and the prevalence of taxa viewed as being more stress tolerant and slower growing (Fanin et al., 2019; Chen et al., 2021). Of note, was the greater abundance of fungi in the phyllosphere soil, while it remained below the limit of detection in soil devoid of plants. The latter is in accordance with Kusch et al. (2020) and Shen (2020) who showed no evidence for an indigenous active fungal community in non-vegetated soils in the hyperarid core. The abundance of fungi in the phyllosphere soil, however, is supported by studies in non-hyperarid climates where leaves of *D. spicata* have been shown to harbour a wide diversity of fungi involved in the turnover of senescent leaf litter (Eliades et al., 2007; Calabon et al., 2021). Low levels of actinomycetes

were detected in all samples, broadly in agreement with Okoro et al. (2009) who were able to recover significant numbers and diversity of these microorganisms in the Atacama Desert. Clearly, further work is required to further investigate the diversity of the active microbial and mesofaunal communities within these environments. A caveat in our study is associated with the preservation of relic DNA and phospholipids in these soils (i.e., necromass) which may lead to an overestimate of microbial biomass size (Wilhelm et al., 2017; Shen , 2020). It should be clarified, however, that studies on the rate of phospholipid turnover in these soils is lacking and future work is needed to investigate the turnover of biomarkers in hyper-arid soils. We note that no mesofauna were visibly present in any of the soils investigated.

4.4. Soil organic carbon in the hyperarid core of the Atacama Desert

Hyperarid regions of the Atacama Desert generally have low amounts of organic C (SOC), typically ranging from 100-500 mg C kg^{-1} (Fuentes et al., 2022a; Lester et al., 2007) and very low levels of labile organic C (0.2-73 mg C kg^{-1}; Fetcher et al., 2012; Mörchen et al., 2019). Our data is consistent with this showing similarly low levels of organic C (140-210 mg C kg^{-1}) in both vegetated and non-vegetated areas. This suggests that either (i) rates of below-ground organic matter production are very low, (ii) that SOC turnover rates are very high under *D. spicata*, or (iii) that the site has not been vegetated for a long period of time, limiting the net accrual of SOC. It should be noted that these factors are not mutually exclusive with evidence available to support each of them. The biological hotspot studied here is associated with a surface aquifer and on rare occasions ephemeral rivers. It is possible that the older saltpetre or nitrate mines located in the study region (operating between 1880-1920) may have altered the hydrological balance and groundwater level present making it recently suited to plant establishment.

The $\delta^{13}C$ values in the phyllosphere (-13.9 ‰), other soils under plants (-17.6 to -18.1 ‰) and bare soils devoid of plants (-24.8 to -23.7 ‰) are significantly different, but without

differences between the top- and subsoils (Table 2). These results are in accordance with the recent study of Knief et al. (2020) reporting $\delta^{13}C$ values of SOC between -22.7 and -28.0 ‰ in a hyper-aridity gradient of the Atacama Desert showing soil surface $\delta^{13}C$ values for Yungay of -26.2 to -26.9 ‰. Ewing et al. (2008) did show that soil SOC $\delta^{13}C$ ranged from -22.7 and -27.8 ‰ between 1 and 216 cm depth. These authors also suggest that in hyperarid soils, SOC is not a direct function of *in situ* photosynthesis but rather a result of atmospheric deposition of organic C (i.e. that C may therefore originate from outside the Atacama Desert region; see Arenas-Díaz et al., 2022).

If, we set the bare soil C_4 contribution of 9-17% as control (Table 3) and assume that the higher relative amount of C_4-C in the vegetated soils (57-60%) and phyllosphere (>85%) are derived from *D. spicata* post-1920, we estimate an annual C turnover rate of 4.1, 2.2, and 15.9 g C m^{-2} yr^{-1} occurring in these top, surface and phyllosphere of the vegetated soils during the last 100 years. In terms of the turnover of C of the current C stocks, we would be looking for a steady state at turnover times of ~180, ~260 ~120 y for surface, subsurface and phyllosphere soil with plants. Warren-Rhodes et al. (2003) reported values of > 600 y for active organic C cycling by hypolithic communities in wetter sites within the Atacama Desert, increasing to > 3000 y in the driest parts. Ziolkowski et al. (2013) suggested rate of C cycling for endolithic microbial communities in the hyperarid Core of the Atacama Desert to range from decadal to a millennium, the latter at the driest sampled site which was Yungay. Boutton et al. (1998) showed in semi-arid savanna ecosystems, that the mean residence time of SOC increased from ca. 40–100 y in the 0–15 cm depth interval, to ca. 300–500 y in the 15–30 cm interval. The bare soils devoid of plants possessed an 'older' C reservoir being mainly derived from C_3 plants, which were present in the past more humid times or originate from long-term atmospheric inputs being conserved in the soil (Ewing et al., 2006; 2008).

Total and dissolved organic C alongside phenolic substances were significantly higher in the phyllosphere soil relative to the other soil samples. This was expected as phenolic

compounds are frequently produced by plants in response to oxidative stress and high salinity (Lopes et al., 2021; Morales-Tapia et al., 2021; Zhang et al., 2022). In addition, the low intrinsic levels of microbial activity and physical protection against UV irradiation may have enhanced their persistence in this soil component. The high levels of phenolics may also have suppressed exoenzyme activity and thus microbial activity (Holik et al., 2017). This is evidenced by near-intact plant litter being found in the phyllosphere soil (Fig. S9). Our data on N availability in the phyllosphere soil also suggest that decomposition is not N limited, despite the high C-to-N ratio of the plant litter.

4.6. Microbial processing of organic C in the hyperarid core of the Atacama Desert

The highest rates of substrate-C mineralization were observed in the soil under plants, presumably due to the higher intrinsic microbial biomass, moisture content and reduced salinity (Jones et al., 2018). It is also likely that a greater proportion of the microbial community was active due to the recent addition of C via rhizodeposition (Pathak and Rao, 1998). This is supported by the much higher mineralization rates in the vegetated topsoil when expressed on a microbial biomass basis. The mineralization data also indicated that small addition of substrate (10 µM glucose), designed to reflect natural concentrations in the rhizosphere from root exudation (Jones et al., 2009), were rapidly utilized by the microbial community. Using a double exponential kinetic modelling approach to describe substrate turnover (Glanville et al., 2016), we estimate that the half-life of ^{14}C-glucose in soil under the vegetated plants was short and ranged from 2-11 h (Table S5), albeit much slower than in temperate soils (Glanville et al., 2016; Hill et al., 2008). A similar calculation was not possible for the bare soils due to the poor model fit, probably reflecting the lag phase in mineralization reflecting the activation and/or growth of the microbial community. As expected, higher concentrations of glucose were mineralized much more slowly. This was particularly apparent in the bare soils where the very long lag phase suggested that the microbial community was too small to process the available-

C or that there were insufficient other resources (e.g., P) to facilitate assimilation. Surprisingly, very low rates of microbial activity were observed in the phyllosphere soil with some samples exhibiting almost no measurable microbial activity. We ascribe this to the origin of the soil material which we believe is predominantly windblown and captured in the plant canopy. This process may be enhanced under high humidity conditions (i.e. fogs) which dissolve the salt crystals and make them conducive to soil binding (data not presented). While on the soil surface prior to transportation, this windblown material is likely to have experienced intense UV irradiation and temperature extremes, effectively sterilizing the material. It should be noted, however, that radioresistant bacteria have been identified in desert sands from other regions of the world suggesting that they may also be present in the Atacama Desert (An et al., 2013; Liu et al., 2022). Our results also suggests that a large proportion of the PLFAs observed in the phyllosphere soil may not reflect an active microbial population but moreover preserved necromass. Further studies using stable isotope probing or transcriptomics should therefore be used to better elucidate the active microbial fraction in these soils. Our studies with plant litter clearly indicate that complex substrates are broken down much more slowly than simple C metabolites such as glucose. This suggests that the presence of microbial ectoenzymes and the subsequent breakdown of complex polymers (e.g., cellulose, protein) into readily assimilatable oligomer units represents the rate limiting step in C turnover in these soils (Jones et al., 2018).

Generally, the values for microbial CUE were relatively similar between the vegetated and unvegetated soils and for the low and high doses of glucose (CUE = 0.30-0.55). However, the values were much lower than reported for other parts of the world using the same glucose concentration (CUE = 0.55-0.75; Jones et al., 2018). This indicates that the hyperarid microbial community is allocating less C towards cell maintenance and the generation of new biomass, but rather partitioning C into more energy intensive processes. We hypothesize that this will be associated with the creation of osmoprotectants, operation of efflux pumps, the need to reduce NO_3^- to NH_4^+ to acquire N, and processes associated with acquiring P from soil (e.g.,

release of phosphatases, organic acids)(Miller and Wood, 1996; Meng et al., 2018; Ameen et al., 2019). This allocation to catabolic processes was greatest in the vegetated soil when supplied with a large amount of glucose-C indicating that microbial growth appears to be inefficient in these hyperarid soils.

4.6. Nitrogen and phosphorus cycling in the hyperarid core of the Atacama Desert

Due to the extremely high NO_3^- concentrations in our soils (1.0 ± 0.2 g kg^{-1}; >2 t N ha^{-1}) we assume that N availability is not limiting microbial activity, rather it is the availability of labile C to firstly reduce NO_3^- to NH_4^+ and the subsequent incorporation of this into organic N compounds (Schaeffer et al., 2003). N cycling will also be limited by the lack of available water and possibly P (Ewing et al., 2008; Jones et al., 2018; Wu et al., 2021). Our findings are consistent with the accumulation of NO_3^- deposits on the soil surface under prolonged hyperarid conditions (Böhlke et al., 1997; Liu et al., 2017). We speculate that the higher amounts of NO_3^- present in the phyllosphere soil are a result of windblown accumulation of $NaNO_3$, as there is no evidence that *D. spicata* or any other plant to our knowledge can actively excrete NO_3^- from its leaves. Our analysis of the salt crystals on the leaf surface also showed no evidence for the presence of NO_3^- (data not shown). Comparison of the fresh and senesced leaves suggests a N, P and K re-assimilation rate of 55, 40 and 72%, respectively, suggesting tight nutrient cycling within the plant, especially for P which is low in the soils examined here (Aerts, 1996). It should be noted that that the buffer power (B_p) values for the non-phyllosphere soils are very high, supporting our measurements of very low bioavailability of P in soil (McDowell et al., 2023). We ascribe this to the strong association of P with minerals such as $CaSO_4$ and the formation of poorly soluble Ca-P minerals, combined with the strongly alkaline soil pH (Guidry et al., 2003; Shen et al., 2020). However, our results also suggest that the presence of plants is leading to a change in the size of the bioavailable P pools as evidenced by

a depletion of the Olsen-P pool and a large net accumulation of P in the acid soluble pool. The latter P pool is likely to be recoverable by plants via organic acid exudation (Jones et al., 2009)

To our knowledge this is the first report of NH_3 emissions occurring during the microbial processing of organic-N in the Atacama Desert. This represents another potential N loss pathway alongside denitrification (Wu et al., 2021). We ascribe this response to the low C:N ratio of arginine which drives microbial ammonification. After microbial uptake, a significant proportion of the arginine-derived C is used in catabolic processes with the excess NH_4^+ excreted back into the soil, where the high pH subsequently promotes NH_3 volatilization. This production of NH_3, however, may benefit other organisms with the capability to scavenge NH_3 from the soil atmosphere (Lynch et al., 2014).

The $\delta^{15}N$ in the phyllosphere was significantly higher (10.0 ‰) than in the soil samples (7.0-7.7 ‰). Similar soil $\delta^{15}N$ values were reported by Díaz et al. (2016), especially for their most hyperarid sites (9.8-10.2 ‰). These authors suggested different mechanisms to explain these high positive $\delta^{15}N$ values in these dry sites, including high N volatilization during elevated diurnal temperatures associated with very alkaline soils or formation of large pools of inorganic N as nitrate.

5. Conclusions

The Atacama Desert represents one of the most extreme places for life to establish on the planet. Within this study, we highlight the extreme climatic and edaphic conditions that exist in the hyperarid core of the Atacama Desert and how these might constrain life within the region. Despite these limitations, however, we demonstrate how the plant *D. spicata* has overcome these to promote plant establishment within the region. Specifically, *D. spicata* appears to physically, chemically and biologically reengineer the system to relieve edaphic and climate stresses. Further, we demonstrate that *D. spicata* accelerates biogeochemical cycling. We also identify that the conversion of NH_4^+ to NH_3 during organic N turnover may represent

a major N loss pathway within these desert ecosystems. In contrast to most ecosystems which are N limited, we show that microbial activity is not constrained by N, but rather by the availability of C and P. Despite the presence of plants, the net gain of soil organic C appears very low, suggesting that C turnover in these biological hotspots is high. In this context, further work is also required to better understand the active component of the rhizosphere microbial community and its functional role in promoting plant success. For example, numerous plant and microbial strategies exist to make P more bioavailable in soil (e.g. mycorrhizas, phosphatases, H^+ and organic acid anion release, increased root hair density, transporter upregulation; Lambers, 2022), however, the relative importance of these and co-benefits for acquisition of water and other nutrients in hyperarid soil remains unknown and should be the subject of future study. In this study we used PLFAs to measure the size and structure of the soil microbial community, however, as noted above, this approach has its drawbacks and provides no information on key microbial taxa which may be influenced by *D. spicata* (e.g. mesofauna, archaea etc). It would therefore be desirable to combine the use of ^{13}C-labelled substrates and compound-specific isotope ratio mass spectrometry (IRMS) to detect which PLFA-taxa were most enriched and therefore of greatest functional significance in carbon turnover (Broughton et al., 2015). Similarly, metagenomic approaches, metabarcoding and ^{18}O labelling may provide insights at a much deeper taxonomic level (Morris et al., 2022). The work undertaken here on NH_3 emissions showed the potential for N to be lost from soil, however, it would be desirable to measure this in the field. Lastly, perchlorates (ClO_4^-) and iodates (IO_3^-) are often present in high concentrations in soils from the Atacama Desert (Catling et al., 2010; Calderon et al., 2014; Lybrand et al., 2016), however, their role in regulating biological activity and biogeochemical cycling remains largely unknown. Further work should therefore focus on potential plant and microbial adaptive strategies to coping with these oxyanions and their potential for abiotic catalysis of C turnover.

773 The hyperarid soils of the Atacama Desert are often used as an analogue of the
774 soils/regolith which might occur on Mars and exoplanets (Navarro-González et al., 2003;
775 Azúa-Bustos et al., 2022). However, evidence suggests that the soils of Mars are composed
776 largely of volcanic basaltic rocks, fine dust, and a variety of mineral oxides and are rich in Fe
777 and Mg, while those of the Atacama Desert are primarily composed of weathered rocks, sand,
778 clay, and salts. In addition, the surface of Mars is subject to greater extremes in temperature,
779 higher levels of radiation and low atmospheric pressure (Galletta et al., 2007; 2009). It would
780 be desirable to investigate how organisms present in our hyperarid Atacama Desert soils
781 respond to conditions which simulate the surface of Mars. Similarly, *D. spicata* may be a good
782 model higher plant to investigate the potential for establishing vegetation on Mars, potentially
783 using replica Martian soils (Kral et al., 2003).
784

785 **Acknowledgements**

786 This work was funded by the UK Biotechnology and Biological Sciences Research Council
787 (BB/N013204/1), Chilean ANID MEC-80190012 project and the ABCJ Geoverbund, German
788 Science Foundation (DFG) as part of CRC1211, Helmholtz Association grant 2173 “Toward a
789 Sustainable Bioeconomy - Resources, Utilization, Engineering and Agroecosystems” (POF
790 IV:2021-2026). We thank Francisco A. Gomez-Valenzuela for help in the field and Anna Ray
791 and Emily Cooledge for help in running the laboratory experiments. We thank Sarah Eppley at
792 Portland State University and James Richards at UC Davis for their insights on the morphology
793 and genetics of *D. spicata*.
794

795 **Declaration of competing interest**

796 The authors declare that they have no known competing financial interests or personal
797 relationships that could have appeared to influence the work reported in this paper.
798

Data availability

Data will be made available on request.

Appendix A. Supplementary data

See attached file.

CRediT author statement

Conceptualization, DLJ, RB, FAD, BF; Methodology DLJ, FAD, RB, RvH, BSA; Investigation, DLJ, FAD, RvH, BSA; Resources BSA, SJM, DLJ, FAD; Data Curation, DLJ, RvH, FAD; Writing – Original Draft, DLJ; Writing - Review & Editing, BF, FAD, DLJ, FR, SJM, RB; Supervision, BF, FR, RB; Funding acquisition, DLJ, BF, FR, RB.

References

Aerts, R., 1996. Nutrient resorption from senescing leaves of perennials: Are there general patterns? Journal of Ecology 84, 597-608. https://doi.org/10.2307/2261481

Alfaro, F.D., Manzano, M., Almiray, C., Garcia, J.L., Osses, P., del Rio, C., Vargas, C., Latorre, C., Koch, M.A., Siegmund, A., Abades, S., 2021. Soil bacterial community structure of fog-dependent *Tillandsia landbeckii* dunes in the Atacama Desert. Plant Systematics and Evolution 307, 56. https://doi.org/10.1007/s00606-021-01781-0

Allen, E.B., Cunningham, G.L., 1983. Effects of vesicular-arbuscular mycorrhizae on *Distichlis spicata* under three salinity levels. New Phytologist 93, 227-236. https://doi.org/10.1111/j.1469-8137.1983.tb03427.x

Ameen, F., AlYahya, S.A., AlNadhari, S., Alasmari, H., Alhoshani, F., Wainwright, M., 2019. Phosphate solubilizing bacteria and fungi in desert soils: species, limitations and

mechanisms. Archives of Agronomy and Soil Science 65, 1446-1459. https://doi.org/10.1080/03650340.2019.1566713

Amundson, R., Dietrich, W., Bellugi, D., Ewing, S., Nishiizumi, K., Chong, G., Owen, J., Finkel, R., Heimsath, A.M., Stewart, B., Caffee, M., 2012. Geomorphologic evidence for the late Pliocene onset of hyperaridity in the Atacama Desert. Bulletin of the Geological Society of America 124, 1048-1070. https://doi.org/10.1130/B30445.1

An, S., Couteau, C., Luo, F., Neveu, J., DuBow, M.S., 2013. Bacterial diversity of surface sand samples from the Gobi and Taklamaken Deserts. Microbial Ecology 66, 850-860. https://doi.org/10.1007/s00248-013-0276-2

Araya, J.P., Gonzalez, M., Cardinale, M., Schnell, S., Stoll, A., 2020. Microbiome dynamics associated with the Atacama flowering desert. Frontiers in Microbiology 10, 3160. https://doi.org/10.3389/fmicb.2019.03160.

Arenas-Díaz, F., Fuentes, B., Reyers, M., Fiedler, S., Böhm, C., Campos, E., Shao, Y., Bol, B., 2022. Dust and aerosols in the Atacama Desert. Earth-Science Reviews 226, 103925. https://doi.org/10.1016/j.earscirev.2022.103925.

Armas, C., Padilla, F.M., Pugnaire, F.I., Jackson, R.B., 2010. Hydraulic lift and tolerance to salinity of semiarid species: consequences for species interactions. Oecologia 162, 11–21. https://doi.org/10.1007/s00442-009-1447-1

Arndt, H., Ritter, B., Rybarski, A., Schiwitza, S., Dunai, T., Nitsche, F., 2020. Mirroring the effect of geological evolution: Protist divergence in the Atacama Desert. Global and Planetary Change 190, 103193. https://doi.org/10.1016/j.gloplacha.2020.103193

Azúa-Bustos, A., González-Silva, C., Mancilla, R. A., Salas, L., Gómez-Silva, B., McKay, C. P., Vicuña, R., 2011. Hypolithic cyanobacteria supported mainly by fog in the coastal range of the Atacama Desert. Microbial Ecology 61, 568-581. http://www.jstor.org/stable/41489079

Azúa-Bustos, A., Urrejola, C., Vicuña, R., 2012. Life at the dry edge: Microorganisms of the Atacama Desert. FEBS Letters 586, 2939-2945. https://doi.org/10.1016/j.febslet.2012.07.025

Azúa-Bustos, A., Caro-Lara, L., Vicuña, R., 2015. Discovery and microbial content of the driest site of the hyper-arid Atacama Desert, Chile. Environmental Microbiology Reports 7, 388-394. https://doi.org/10.1111/1758-2229.12261

Azúa-Bustos, A., González-Silva., C., Fairén, A.G., 2022. The Atacama Desert in Northern Chile as an analog model of Mars. Frontiers in Astronomy and Space Science 8, 810426. https://doi.org/10.3389/fspas.2021.810426

Balesdent, J., Mariotti, A., Guillet, B., 1987. Natural ^{13}C abundance as a tracer for studies of soil organic matter dynamics. Soil Biology and Biochemistry 19, 25-30. https://doi.org/10.1016/0038-0717(87)90120-9

Barber, S.A., 1995. Soil Nutrient Bioavailability: A Mechanistic Approach, 2nd Edition. John Wiley & Sons, New York. ISBN: 978-0-471-58747-7

Bazihizina, N., Veneklaas, E.J., Barrett-Lennard, E.G., Colmer, T.D., 2017. Hydraulic redistribution: limitations for plants in saline soils. Plant, Cell & Environment 40, 2437–2446. https://doi.org/10.1111/pce.13020

Böhlke, J.K., Ericksen, G.E., Revesz, K., 1997. Stable isotope evidence for an atmospheric origin of desert nitrate deposits in northern Chile and southern California, U.S.A. Chemical. Geology 136, 135-152. https://doi.org/10.1016/S0009-2541(96)00124-6

Boutton, T.W., Archer, S.R., Midwood, A.J., Zitzer, S.F., Bol, R., 1998. $\delta^{13}C$ values of soil organic carbon and their use in documenting vegetation change in a subtropical savanna ecosystem. Geoderma 82, 5-41. https://doi.org/10.1016/S0016-7061(97)00095-5

Brewer, J.S., Bertness, M.D., 1996. Disturbance and intraspecific variation in the clonal morphology of salt marsh perennials. Oikos 77, 107-116. https://doi.org/10.2307/3545590

874 Broughton, R.C.I., Newsham, K.K., Hill, P.W., Stott, A., Jones, D.L., 2015. Differential
875 acquisition of amino acid and peptide enantiomers within the soil microbial community
876 and its implications for carbon and nitrogen cycling in soil. Soil Biology and
877 Biochemistry 88, 83-89. https://doi.org/10.1016/j.soilbio.2015.05.003.
878 Buyer, J.S., Sasser, M., 2012. High throughput phospholipid fatty acid analysis of soils.
879 Applied Soil Ecology 61, 127-130. https://doi.org/10.1016/j.apsoil.2012.06.005
880 Cáceres, L., Gomez-Silva, B., Garró, X., Rodriguez, V., Monardes, V., McKay, C.P., 2007.
881 Relative humidity patterns and fog water precipitation in the Atacama Desert and
882 biological implications. Journal of Geophysical Research Biogeosciences 112, G04S14.
883 https://doi.org/10.1029/2006JG000344
884 Calabon, M.S., Jones, E.B.G., Promputtha, I., Hyde, K.D., 2021. Fungal biodiversity in salt
885 marsh ecosystems. Journal of Fungi 7, 648. https://doi.org/10.3390/jof7080648
886 Calderon, R.,Palma, P., Parker, D., Molina, M., Godoy, F.A., Escudey, M.P., 2014.
887 Perchlorate levels in soil and waters from the Atacama Desert. Archives of
888 Environmental Contamination and Toxicology 66, 155-161.
889 https://doi.org/10.1007/s00244-013-9960-y
890 Castillo, R.V., Stanton, D., Nelson, P.R., 2017. Contributions to the knowledge of the lichen
891 biota of the mist oasis of Alto Patache, Atacama Desert. Revista de Geografía Norte
892 Grande 68, 49-64. https://doi.org/10.4067/S0718-34022017000300049
893 Catling, D.C., Claire, M.W., Zahnle, K.J., Quinn, R.C., Clark, B.C., Hecht, M.H., Kounaves,
894 S., 2010. Atmospheric origins of perchlorate on Mars and in the Atacama. Journal of
895 Geophysical Research-Planets 115, E00E11. https://doi.org/10.1029/2009JE003425
896 Chen, C., Chen, H.Y.H., Chen, X., Huang, Z., 2019. Meta-analysis shows positive effects of
897 plant diversity on microbial biomass and respiration. Nature Communications 10, 1332.
898 https://doi.org/10.1038/s41467-019-09258-y

899 Colmer, T.D., Flowers, T.J., 2008. Flooding tolerance in halophytes. New Phytologist 179,
900 964–974. https://doi.org/10.1111/j.1469-8137.2008.02483.x
901 Compant, S., Samad, A., Faist, H., Sessitsch, A., 2019. A review on the plant microbiome:
902 Ecology, functions, and emerging trends in microbial application. Journal of Advanced
903 Research 19, 29-37. https://doi.org/10.1016/j.jare.2019.03.004
904 Cordero, R. R., Damiani, A., Jorquera, J., Sepúlveda, E., Caballero, M., Fernandez, S., Feron,
905 P., Llanillo, J., Carrasco, D., Laroze, L., Labbe, F., 2018. Ultraviolet radiation in the
906 Atacama Desert. Antonie Van Leeuwenhoek, 111, 1301-1313.
907 https://doi.org/10.1007/s10482-018-1075-z
908 Dawson, T.E., 1993. Hydraulic lift and water use by plants: implications for water balance,
909 performance and plant-plant interactions. Oecologia 95, 565–574.
910 https://doi.org/10.1007/bf00317442
911 de Groot, P.A., 2004. Handbook of Stable Isotope Analytical Techniques. Volume 1. Elsevier
912 Science Ltd, Amsterdam, The Netherlands. ISBN 978-0-444-51114-0
913 Diefendorf, A.F., Mueller, K.E., Wing, S.L., Koch, P.L. and Freeman, K.H., 2010. Global
914 patterns in leaf ^{13}C discrimination and implications for studies of past and future
915 climate. Proceedings of the National Academy of Sciences 107, 5738-5743.
916 https://www.pnas.org/doi/full/10.1073/pnas.0910513107
917 Eliades, L.A., Voget, C.E., Arambarri, A.M., Cabello, M.N., 2007. Fungal communities on
918 decaying saltgrass (*Distichlis spicata*) in Buenos Aires province (Argentina). Sydowia
919 59, 227-234.
920 Eppley, S.M, Mercer, C.A., Haaning, C., Graves, C.B., 2009. Sex-specific variation in the
921 interaction between *Distichlis spicata* (Poaceae) and mycorrhizal fungi. American
922 Journal of Botany 96, 1967-1973. https://doi.org/10.3732/ajb.0900076

Ewing, S. A., Macalady, J. L., Warren-Rhodes, K., McKay, C. P., Amundson, R., 2008. Changes in the soil C cycle at the arid-hyper-arid transition in the Atacama Desert. Journal of Geophysical Research 113, G02S90. https://doi.org/10.1029/2007JG000495.

Ewing, S.A., Sutter, B., Owen, J., Nishiizumi, K., Sharp, W., Cliff, S.S., Perry, K., Dietrich, W., McKay, C.P., Amundson, R., 2006. A threshold in soil formation at Earth's arid-hyper-arid transition. Geochimica et Cosmochimica Acta 70, 5293-5322. https://doi.org/10.1016/j.gca.2006.08.020

Fanin, N., Kardol, P., Farrell, M., Nilsson, M.C., Gundale, M.J., Wardle, D.A., 2019. The ratio of Gram-positive to Gram-negative bacterial PLFA markers as an indicator of carbon availability in organic soils. Soil Biology and Biochemistry 128, 111-114. https://doi.org/10.1016/j.soilbio.2018.10.010

FAO, 2021. Standard operating procedure for soil available phosphorus - Olsen method. Food and Agriculture Organization of the United Nations, Rome.

Ferrando, R., Espinoza, F., 2013. Mapa geología "Carta Aguas Blancas" (escala 1:100.000), región de Antofagasta, Chile. https://www.researchgate.net/publication/359377967_Mapa_geologia_Carta_Aguas_Blancas_escala_1100000_region_de_Antofagasta_Chile#fullTextFileContent

Findlay, R.H., 2004. Determination of microbial community structure using phospholipid fatty acid profiles. Molecular Microbial Ecology Manual 4, 983-1004. https://doi.org/10.1007/978-1-4020-2177-0_408

Finstad, K., Pfeiffer, M., Amundson, R., 2014. Hyperarid soils and the soil taxonomy. Soil Science Society of America Journal 78, 1845-1851. https://doi.org/10.2136/sssaj2014.06.0247

Fletcher, L.E., Valdivia-Silva, J.E., Pérez-Montaño, S., Condori-Apaza, R.M., Conley, C.A., McKay, C.P., 2012. Variability of organic material in surface horizons of the hyper-arid

948 Mars-like soils of the Atacama Desert. Advances in Space Research 49, 271-279.
949 https://doi.org/10.1016/j.asr.2011.10.001
950 Flowers, T.J., Colmer, T.D., 2015. Plant salt tolerance: adaptations in halophytes. Annals of
951 Botany 115, 327-331. https://doi.org/10.1093/aob/mcu267
952 Frostegard, A., Bååth, E., 1996. The use of phospholipid fatty acid analysis to estimate
953 bacterial and fungal biomass in soil. Biology and Fertility of Soils 22, 59-65.
954 https://doi.org/10.1007/BF00384433
955 Frostegård, Å., Bååth, E., Tunlid, A., 1993. Shifts in the structure of soil microbial
956 communities in limed forests as revealed by phospholipid fatty acid analysis. Soil
957 Biology and Biochemistry 25, 723-730. https://doi.org/10.1016/0038-0717(93)90113-P
958 Fuentes, B., Gómez, F., Valdez, C., Videla, A., Castro-Severyn, J., Barahona, S., Bol, R.,
959 Riquelme R., Quispe, J., Remonsellez, F., 2022a. Effects of altitude on soil properties
960 in coastal fog ecosystems in Morro Moreno National Park, Antofagasta, Chile.
961 European Journal of Soil Science 73, e13217. https://doi.org/10.1111/ejss.13217
962 Fuentes, B., Choque, A., Gómez, F., Alarcón, A., Castro-Nallar, E., Arenas, F., Contreras, D.,
963 Mörchen, R., Amelung, W., Knief, C., Moradi, G., Klumpp, E., Saavedra, C.P.,
964 Prietzel, J., Klysubun, W., Remonsellez, F., Bol, R., 2022b. Influence of physical-
965 chemical soil parameters on microbiota composition and diversity in a deep hyper-arid
966 core of the Atacama Desert. Frontiers in Microbiology 12, 794743.
967 https://doi.org/10.3389/fmicb.2021.794743
968 Galletta, G., Ferri, F., Fanti, G., D'Alessandro, M., Bertoloni, G., Pavarin, D., Bettanini, C.,
969 Cozza, P., Pretto, P., Bianchini, G., Debei, S., 2007. S.A.M., the Italian Martian
970 Simulation Chamber. Origins of Life and Evolution of Biospheres 36, 625–627.
971 https://doi.org/10.1007/s11084-006-9046-1

Galletta, G., D'Alessandro, M., Bertoloni, G., Castellani, F., 2009. Surviving on Mars: test with LISA simulator. Proceedings of the International Astronomical Union 5, 686–687. https://doi.org/10.1017/s1743921310010951

Gao, Y., Tariq, A., Zeng, F., Sardans, J., Peñuelas, J., Zhang, Z., Islam, W., Xu, M., 2022. Fertile islands" beneath three desert vegetation on soil phosphorus fractions, enzymatic activities, and microbial biomass in the desert-oasis transition zone. Catena, 212, 106090. https://doi.org/10.1016/j.catena.2022.106090

Garner, W., Steinberger, Y., 1989. A proposed mechanism for the formation of 'Fertile Islands' in the desert ecosystem. Journal of Arid Environments 16, 257-262. https://doi.org/10.1016/S0140-1963(18)30941-8

Glanville, H.C., Hill, P.W., Maccarone, L.D., Golyshin, P.N., Murphy, D.V., Jones, D.L., 2012. Temperature and water controls on vegetation emergence, microbial dynamics, and soil carbon and nitrogen fluxes in a high Arctic tundra ecosystem. Functional Ecology 26, 1366-1380. https://doi.org/10.1111/j.1365-2435.2012.02056.x

Glanville, H.C., Hill, P.W., Schnepf, A., Oburger, E., Jones, D.L., 2016. Combined use of empirical data and mathematical modelling to better estimate the microbial turnover of isotopically labelled carbon substrates in soil. Soil Biology and Biochemistry 94, 154-168. https://doi.org/10.1016/j.soilbio.2015.11.016

Golden, A.M., Baldwin, J.G., Mundo-Ocampo, M., 1995. Description of *Tylenchorhynchus thermophilus* n. sp. (Nematoda: Tylenchina) from saltgrass in Death Valley, California. Journal of Nematology 27, 312-319.

Guidry, M.W., Mackenzie, F.T., 2003. Experimental study of igneous and sedimentary apatite dissolution: control of pH, distance from equilibrium, and temperature on dissolution rates. Geochimica et Cosmochimica Acta 67, 2949–2963. https://doi.org/10.1016/S0016-7037(03)00265-5

997 Hansen, D.J., Dayanadan, P., Kaufman, P.B., Brotherson, J.D., 1976. Ecological adaptations
998 of salt-marsh grass, *Distichlis spicata* (Graminae), and environmental factors affecting
999 its growth and distribution. American Journal of Botany 63, 635-650.
1000 https://doi.org/10.2307/2441826
1001 Hasanuzzaman, M., Nahar, K., Alam, M.M., Bhowmik, P.C., Hossain, M.A., Rahman, M.M.,
1002 Prasad, M.N., Ozturk, M., Fujita, M., 2014. Potential use of halophytes to remediate
1003 saline soils. BioMed Research International 2014, 589341.
1004 https://doi.org/10.1155/2014/589341
1005 Hill, P.W., Marshall, C., Williams, G.G., Blum, H., Harmens, H., Jones, D.L., Farrar, J.F.,
1006 2007. The fate of photosynthetically-fixed carbon in *Lolium perenne* L. grassland as
1007 modified by elevated CO_2 and sward management. New Phytologist 173, 766-777.
1008 https://doi.org/10.1111/j.1469-8137.2007.01966.x
1009 Hill, P.W., Farrar, J.F., Jones, D.L., 2008. Decoupling of microbial glucose uptake and
1010 mineralization in soil. Soil Biology and Biochemistry 40, 616-624.
1011 https://doi.org/10.1016/j.soilbio.2007.09.008
1012 Holik, L., Vranova, V., Rosikova, J., Rejsek, K., 2017. Protease activity of forest soils and
1013 their responses to phenolic compounds in soil. Chemicke Listy 111, 47-49.
1014 Ingendesa, 1997. Proyecto Aguas Blancas, Estudio de Impacto Ambiental. Expediente
1015 consolidado. Available in
1016 https://seia.sea.gob.cl/expediente/expedientesEvaluacion.php?id_expediente=315&idEx
1017 pediente=315
1018 Jones, D.L., Nguyen, C., Finlay, R.D., 2009. Carbon flow in the rhizosphere: carbon trading
1019 at the soil-root interface. Plant and Soil 321, 5-33. https://doi.org/10.1007/s11104-009-
1020 9925-0
1021 Jones, D.L., Olivera-Ardid, S, Klumpp, E, Knief, C., Hill, P.W., Lehndorff, E., Bol, R.,
1022 2018a. Moisture activation and carbon use efficiency of soil microbial communities

1023 along an aridity gradient in the Atacama Desert. Soil Biology and Biochemistry 117,
1024 68-71. https://doi.org/10.1016/j.soilbio.2017.10.026
1025 Jones, D.L., Hill, P.W., Smith, A.R., Farrell, M., Ge, T., Banning, N.C., Murphy, D.V.,
1026 2018b. Role of substrate supply on microbial carbon use efficiency and its role in
1027 interpreting soil microbial community-level physiological profiles (CLPP). Soil
1028 Biology and Biochemistry 123, 1-6. https://doi.org/10.1016/j.soilbio.2018.04.014
1029 Kaiser, C., Frank, A., Wild, B., Koranda, M., Richter, A., 2010. Negligible contribution from
1030 roots to soil-borne phospholipid fatty acid fungal biomarkers 18:2ω6,9 and 18:1ω9.
1031 Soil Biology & Biochemistry 42, 1650–1652.
1032 https://doi.org/10.1016/j.soilbio.2010.05.019
1033 Kemmitt, S.J., Wright, D., Goulding, K.W.T., Jones, D.L., 2006. pH regulation of carbon and
1034 nitrogen dynamics in two agricultural soils. Soil Biology and Biochemistry 38, 898-
1035 911. https://doi.org/10.1016/j.soilbio.2005.08.006
1036 Kidron, G.J., 2009. The effect of shrub canopy upon surface temperatures and evaporation in
1037 the Negev Desert. Earth Surface Processes and Landforms 34, 123-132.
1038 https://doi.org/10.1002/esp.1706
1039 Knief, C., Bol, R., Amelung, W., Kush, S., Frindte, K., Eckmeier, E., Jaeschke, A., Dunai, T.,
1040 Fuentes, B., Mörchen, R., Schütte, T., Lücke, A., Klumpp, E., Kaiser, K., Rethemeyer,
1041 J., 2020. Tracing elevational changes in microbial life and organic carbon sources in
1042 soils of the Atacama Desert. Global and Planetary Change 184, 103078.
1043 https://doi.org/10.1016/j.gloplacha.2019.103078
1044 Kohn, M.J., 2010. Carbon isotope compositions of terrestrial C3 plants as indicators of
1045 (paleo) ecology and (paleo) climate. Proceedings of the National Academy of Sciences,
1046 107, 19691-19695. https://www.pnas.org/doi/full/10.1073/pnas.1004933107

1047 Kral, T.A., Bekkum, C.R., Mckay, C.P., 2004. Growth of methanogens on a Mars soil
1048 simulant. Origins of Life and Evolution of Biospheres 34, 615–626.
1049 https://doi.org/10.1023/b:orig.0000043129.68196.5f
1050 Kusch, S., Jaeschke, A., Morchen, R., Rethemeyer, J., 2020. Tracing life at the dry limit
1051 using phospholipid fatty acids - does sampling matter? Soil Biology and Biochemistry
1052 141, 107661. https://doi.org/10.1016/j.soilbio.2019.107661
1053 Lambers, H., 2022. Phosphorus acquisition and utilization in plants. Annual Review of Plant
1054 Biology 73, 17-42. https://doi.org/10.1146/annurev-arplant-102720-125738
1055 Lazarus, B.E., Richards, J.H., Gordon, P.E., Oki, L.R., Barnes, C.S., 2011. Plasticity
1056 tradeoffs in salt tolerance mechanisms among desert *Distichlis spicata* genotypes.
1057 Functional Plant Biology 38, 187-198. https://doi.org/10.1071/FP10192
1058 Lester, E. D., Satomi, M., Ponce, A., 2007. Microflora of extreme arid Atacama Desert soils.
1059 Soil Biology and Biochemistry 39, 704-708.
1060 https://doi.org/10.1016/j.soilbio.2006.09.020
1061 Litalien, A.A., Raymond, W.D., Rutter, A., Zeeb, B.A., 2020. Development of a model for
1062 the dispersal of salts from recretohalophytes. ACS Earth and Space Chemistry 4, 1367–
1063 1374. https://doi.org/10.1021/acsearthspacechem.0c00080
1064 Liu, D., Zhu, W., Wang, X., Pan, Y., Wang, C., Xi, D., Bai, E., Wang Y., 2017. Abiotic
1065 versus biotic controls on soil nitrogen cycling in drylands along a 3200 km transect.
1066 Biogeosciences 14, 989-1001. https://doi.org/10.5194/bg-14-989-2017
1067 Liu, Y., Chen, T., Li, J., Wu, M.H., Liu, G.X., Zhang, W., Zhang, B.L., Zhang, S.L., Zhang,
1068 G.S., 2022. High proportions of radiation-resistant strains in culturable bacteria from
1069 the Taklimakan Desert. Biology 11, 501. https://doi.org/10.3390/biology11040501
1070 Liu, J.Q., Sun, X., Zuo, Y.L., Hu, Q.N., He, X.L., 2023. Plant species shape the bacterial
1071 communities on the phyllosphere in a hyper-arid desert. Microbiological Research 269,
1072 127314. https://doi.org/10.1016/j.micres.2023.127314

1073 Lopes, M., Sanches-Silva, A., Castilho, M., Cavaleiro, C., Ramos, F., 2021. Halophytes as
1074 source of bioactive phenolic compounds and their potential applications. Critical
1075 Reviews in Food Science and Nutrition 63, 1078-1101.
1076 https://doi.org/10.1080/10408398.2021.1959295
1077 Lybrand, R.A., Bockheim, J.G., Ge, W.S., Graham, R.C., Hlohowskyj, S.R., Michalski, G.,
1078 Prellwitz, J.S., Rech, J.A., Wang, F., Parker, D.R., 2016. Nitrate, perchlorate, and
1079 iodate co-occur in coastal and inland deserts on Earth. Chemical Geology 442, 174-186.
1080 https://doi.org/10.1016/j.chemgeo.2016.05.023
1081 Lynch, R.C., Darcy, J.L., Kane, N.C., Nemergut, D.R., Schmidt, S.K., 2014. Metagenomic
1082 evidence for metabolism of trace atmospheric gases by high-elevation desert
1083 Actinobacteria. Frontiers in Microbiology 5, 698.
1084 https://doi.org/10.3389/fmicb.2014.00698
1085 Marquet, P.A., Bozinovic, F., Bradshaw, G.A., Cornelius, C., Gonzalez, H., Gutierrez, J.R.,
1086 Hajek, E.R., Lagos, J.A., Lopez-Cortes, F., Nunez, L., Rosello, E.F., Santoro, C.,
1087 Samaniego, H., Standen, V.G., Torres-Mura, J.C., Jaksic, F.M., 1998. Ecosystems of
1088 the Atacama Desert and adjacent Andean area in northern Chile. Revista Chilena de
1089 Historia Natural 71, 593-617.
1090 McCray, J.M., Wright, A.L., Luo, Y.G., Ji, S.N., 2012. Soil phosphorus forms related to
1091 extractable phosphorus in the everglades agricultural area. Soil Science 177, 31-38.
1092 https://doi.org/10.1097/SS.0b013e31823782da
1093 McDowell, R.W., Noble, A., Pletnyakov, P., Haygarth, P.M., 2023. A global database of soil
1094 plant available phosphorus. Scientific Data 10, 125. https://doi.org/10.1038/s41597-
1095 023-02022-4
1096 McKay, C.P., Friedmann, E.I., Gómez-Silva, B., Cáceres-Villanueva, L., Andersen, D.T.,
1097 Landheim, R., 2003. Temperature and moisture conditions for life in the extreme arid

region of the Atacama Desert: four years of observations including the El Niño of 1997-1998. Astrobiology 3, 393-406. https://doi.org/10.1089/153110703769016460

Meng, Y.B., Yin, C.Q., Zhou, Z.B., Meng, F.G., 2018. Increased salinity triggers significant changes in the functional proteins of ANAMMOX bacteria within a biofilm community. Chemosphere 207, 655-664. https://doi.org/10.1016/j.chemosphere.2018.05.076

Miller, K.J., Wood, J.M., 1996. Osmoadaptation by rhizosphere bacteria. Annual Review of Microbiology 50, 101-136. https://doi.org/10.1146/annurev.micro.50.1.101

Mintz, Y., Walker, G.K., 1993. Global fields of soil moisture and land surface evapotranspiration derived from observed precipitation and surface air temperature. Journal of Applied Meteorology 32, 1305-34. https://doi.org/10.1175/1520-0450(1993)032<1305:GFOSMA>2.0.CO;2

Miranda, K.M., Espey, M.G., Wink, D.A., 2001. A rapid, simple spectrophotometric method for simultaneous detection of nitrate and nitrite. Nitric Oxide Biology and Chemistry 5, 62-71. https://doi.org/10.1006/niox.2000.0319

Morales-Tapia, P., Cabrera-Barjas, G., Giordano, A., 2021. Polyphenolic distribution in organs of *Argylia radiata*, an extremophile plant from Chilean Atacama desert. Natural Product Research 35, 4143–4147. https://doi.org/10.1080/14786419.2020.1739678

Mörchen, R., Lehndorff, E., Arenas-Díaz, F. Moradi, G., Bol. R., Fuentes, B., Klumpp, E., Amelung, W., 2019. Carbon accrual in the Atacama Desert. Global and Planetary Change 181, 102993. https://doi.org/10.1016/j.gloplacha.2019.102993

Morris, K.A., Richter, A., Migliavacca, M., Schrumpf, M., 2022. Growth of soil microbes is not limited by the availability of nitrogen and phosphorus in a Mediterranean oak-savanna. Soil Biology and Biochemistry 169, 108680. https://doi.org/10.1016/j.soilbio.2022.108680

Morris, L., Yun, K., Rutter, A., Zeeb, B.A., 2019. Characterization of excreted salt from the recretohalophytes *Distichlis spicata* and *Spartina pectinata*. Journal of Environmental Quality 48, 1775–1780. https://doi.org/10.2134/jeq2019.03.0102

Mulvaney, R.L., 1996. Nitrogen- Inorganic forms. In: Sparks, D.L (ed), Methods of Soil Analysis. Part3. Soil Society of America Inc., Madison, WI, pp. 1123-1184.

Napier, J.A., Haslam, R.P., Beaudoin, F., Cahoon, E.B., 2014. Understanding and manipulating plant lipid composition: metabolic engineering leads the way. Current Opinion in Plant Biology 19, 68– 75. https://doi.org/10.1016/j.pbi.2014.04.001

Navarro-Gonzalez, R., Rainey, F.A., Molina, P., Bagaley, D.R., Hollen, B.J., de la Rosa, J., Small, A.M., Quinn, R.C., Grunthaner, F.J., Caceres, L., 2003. Mars-like soils in the Atacama Desert, Chile, and the dry limit of microbial life. Science 302, 1018-1021. https://doi.org/10.1126/science.1089143

Okoro, C.K., Brown, R., Jones, A.L., Andrews, B.A., Asenjo, J.A., Goodfellow, M., Bull, A.T., 2009. Diversity of culturable actinomycetes in hyper-arid soils of the Atacama Desert, Chile. Antonie van Leeuwenhoek 95, 121-133. https://doi.org/10.1007/s10482-008-9295-2

Olsson, P.A., 1999. Signature fatty acids provide tools for determination of the distribution and interactions of mycorrhizal fungi in soil. FEMS Microbiology Ecology 29, 303–310. https://doi.org/10.1111/j.1574-6941.1999.tb00621.x

Pathak, H., Rao, D.L.N., 1998. Carbon and nitrogen mineralization from added organic matter in saline and alkali soils, Soil Biology and Biochemistry 30, 695-702. https://doi.org/10.1016/S0038-0717(97)00208-3

Pfeiffer, M., Morgan, A., Heimsath, A., Jordan, T., Howard, A., Amundson, R., 2021. Century scale rainfall in the absolute Atacama Desert: Landscape response and implications for past and future rainfall. Quaternary Science Reviews 254, 106797. https://doi.org/10.1016/j.quascirev.2021.106797.

1149 Reuss-Schmidt, K., Rosenstiel, T.N., Rogers, S.R., Simpson, A.G., Eppley, S.M., 2015.
1150 Effects of sex and mycorrhizal fungi on gas exchange in the dioecious salt marsh grass
1151 *Distichlis spicata*. International Journal of Plant Sciences 176, 141-149.
1152 https://doi.org/10.1086/679351
1153 Rondanelli, R., Molina, A., Falvey, M., 2015. The Atacama surface solar maximum. Bulletin
1154 of the American Meteorological Society 96, 405-418. https://doi.org/10.1175/BAMS-
1155 D-13-00175.1
1156 Santander, C., Garcia, S., Moreira, J., Aponte, H., Araneda, P., Olave, J., Vidal, G., Cornejo,
1157 P., 2021. Arbuscular mycorrhizal fungal abundance in elevation belts of the hyperarid
1158 Atacama Desert. Fungal Ecology 51, 101060.
1159 https://doi.org/10.1016/j.funeco.2021.101060
1160 Semenova, G.A., Fomina, I.R., Biel, K.Y., 2010. Structural features of the salt glands of the
1161 leaf of *Distichlis spicata* 'Yensen 4a' (Poaceae). Protoplasma 240, 75–82.
1162 https://doi.org/10.1007/s00709-009-0092-1
1163 She, W.W., Chen, N., Zhang, Y.Q., Qin, S.G., Bai, Y.X., Feng, W., Lai, Z.R., Qiao, Y.G.,
1164 Liu, L., Zhang, W.J.,Miao, C., 2022. Precipitation and nitrogen deposition alter
1165 biocrust-vascular plant coexistence in a desert ecosystem: Threshold and mechanisms.
1166 Journal of Ecology 110, 772-783. https://doi.org/10.1111/1365-2745.13834
1167 Shen, J.X., 2020. Phospholipid biomarkers in Mars-analogous soils of the Atacama Desert.
1168 International Journal of Astrobiology 19, 505-514.
1169 https://doi.org/10.1017/S1473550420000294
1170 Shen, J.X., Smith, A.C., Claire, M.W., Zerkle, A.L., 2020. Unraveling biogeochemical
1171 phosphorus dynamics in hyperarid Mars-analogue soils using stable oxygen isotopes in
1172 phosphate. Geobiology 18, 760-779. https://doi.org/10.1111/gbi.12408

1173 Sotomayor, D.A., Drezner, T.D., 2019. Dominant plants alter the microclimate along a fog
1174 gradient in the Atacama Desert. Plant Ecology 220, 417-432.
1175 https://doi.org/10.1007/s11258-019-00924-1
1176 Sutter, B., Dalton, J.B., Ewing, S.A., Amundson, R., Mckay, C.P., 2007. Terrestrial analogs
1177 for interpretation of infrared spectra from the Martian surface and subsurface: Sulfate,
1178 nitrate, carbonate, and phyllosilicate-bearing Atacama Desert soils. Journal of
1179 Geophysical Research Biogeosciences 112, G04S10.
1180 https://doi.org/10.1029/2006JG000313
1181 Trivedi, P., Leach, J.E., Tringe, S.G., Sa, T., Singh, B.K., 2020. Plant-microbiome
1182 interactions: from community assembly to plant health. Nature Reviews Microbiology
1183 18, 607-621. https://doi.org/10.1038/s41579-020-0412-1
1184 UNEP, 1997. World Atlas of Desertification. 2nd edition. United Nations Environmental
1185 Programme, Nairobi, Kenya.
1186 Uritskiy, G., Getsin, S., Munn, A., Gomez-Silva, B., Davila, A., Glass, B., Taylor, J.,
1187 DiRuggiero, J., 2019. Halophilic microbial community compositional shift after a rare
1188 rainfall in the Atacama Desert. ISME Journal 13, 2737-2749.
1189 https://doi.org/10.1038/s41396-019-0468-y
1190 Voigt, C., Klipsch, S., Herwartz, D., Chong, G., Staubwasser, M., 2020. The spatial
1191 distribution of soluble salts in the surface soil of the Atacama Desert and their
1192 relationship to hyperaridity. Global and Planetary Change 184, 103077.
1193 https://doi.org/10.1016/j.gloplacha.2019.103077
1194 Wang, F., Michalski, G., Luo, H., Caffee, M., 2017. Role of biological soil crusts in affecting
1195 soil evolution and salt geochemistry in hyper-arid Atacama Desert, Chile. Geoderma
1196 307, 54-64. https://doi.org/10.1016/j.geoderma.2017.07.035
1197 Waring, S.A., Bremner, J.M., 1964. Ammonium production in soil under waterlogged
1198 conditions as an index of N availability. Nature 201, 951-952.

1199 Warren, R.S., Brockelman, P.M., 1989. Photosynthesis, respiration, and salt gland activity of
1200 *Distichlis spicata* in relation to soil salinity. Botanical Gazette 150, 346-350.
1201 https://www.jstor.org/stable/2995434
1202 Warren-Rhodes, K.A., Rhodes, K.L., Pointing, S.B., Ewing, S.A., Lacap, D.C., Gómez-Silva,
1203 B., Amundson, R., Friedmann, E.I., McKay, C.P., 2006. Hypolithic cyanobacteria, dry
1204 limit of photosynthesis, and microbial ecology in the hyperarid Atacama Desert.
1205 Microbial Ecology 52, 389-398. https://doi:10.1007/s00248-006-9055-7
1206 Warren-Rhodes, K., Ewing, S., McKay, C.P., Rhodes, K.L., 2003. Exploring the limits to
1207 photosynthetic life in the hyperarid Atacama (Chile) and Taklimakan (China) deserts.
1208 American Geophysical Union, Fall Meeting 2003, abstract id. B52B-1042.
1209 Weiler, M., 2005. An infiltration model based on flow variability in macropores:
1210 development, sensitivity analysis and applications. Journal of Hydrology 310, 294-315.
1211 https://doi.org/10.1016/j.jhydrol.2005.01.010.
1212 Wilhelm, M.B., Davila, A.F., Eigenbrode, J.L., Parenteau, M.N., Jahnke, L.L., Liu, X.L.,
1213 Summons, R.E., Wray, J.J., Stamos, B.N., O'Reilly, S.S., 2017. Xeropreservation of
1214 functionalized lipid biomarkers in hyperarid soils in the Atacama Desert. Organic
1215 Geochemistry 103, 97-104. https://doi.org/10.1016/j.orggeochem.2016.10.015
1216 Wu, D., Senbayram, M., Moradi, G., Morchen, R., Knief, C., Klumpp, E., Jones, D.L., Well,
1217 R., Chen, R.R., Bol, R., 2021. Microbial potential for denitrification in the hyperarid
1218 Atacama Desert soils. Soil Biology and Biochemistry 157, 108248.
1219 https://doi.org/10.1016/j.soilbio.2021.108248
1220 Yun, K.B.M., Koster, S., Rutter, A., Zeeb, B.A., 2019. Haloconduction as a remediation
1221 strategy: Capture and quantification of salts excreted by recretohalophytes. Science of
1222 the Total Environment 685, 827–835. https://doi.org/10.1016/j.scitotenv.2019.06.271

Zhang, Y., Cai, P., Cheng, G., Zhang, Y., 2022. A brief review of phenolic compounds identified from plants: their extraction, analysis, and biological activity. Natural Product Communications 17, 1-14. https://doi.org/10.1177/1934578X211069721

Ziolkowski, L.A., Wierzchos, J., Davila, A.F., Slater, G.F., 2013. Radiocarbon evidence of active endolithic microbial communities in the hyperarid core of the Atacama Desert. Astrobiology 13, 607-616. https://doi.org/10.1089/ast.2012.0854

Fig. 1. Temperature and relative humidity of the air in the above-ground plant canopy, soil surface (0-1 cm) and subsurface (10 cm) layers at the field site in the Atacama Desert.

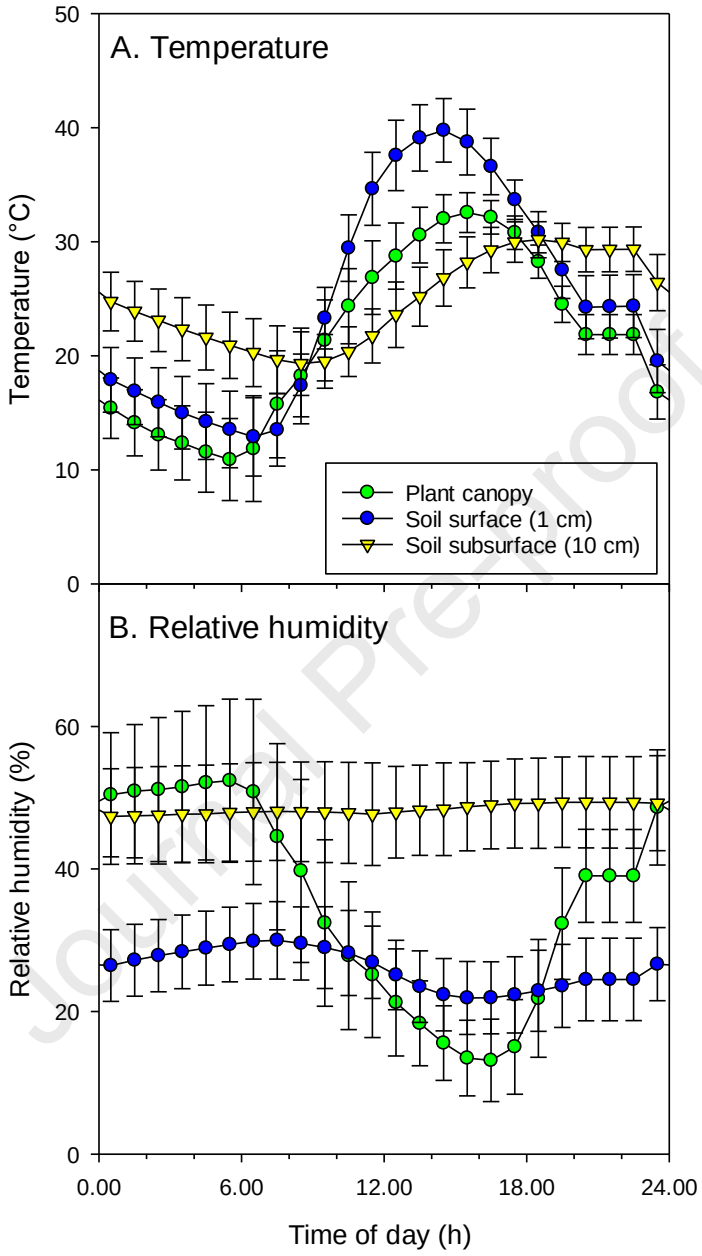

Fig. 2. X-ray scans of soil at the base (0-5 cm depth) of the *D. spicata* plant columns (i) showing the highly cemented (high density) region at the soil surface (sample area in red) and the underlying low-density matrix towards the top half (sample area in green) and the plant material (aerenchymous rhizomes) running through the soil. Bulk soil porosity analysis was performed on the largest possible sample area that could be accommodated due to the shape of the sample (highlighted in blue). (ii) Selected plant material highlighted in purple used as mask for analysis. (iii) 3D bulk volume representative image. (iv) 3D cross-sectional bulk volume showing the ingress of roots/organic matter into the sample.

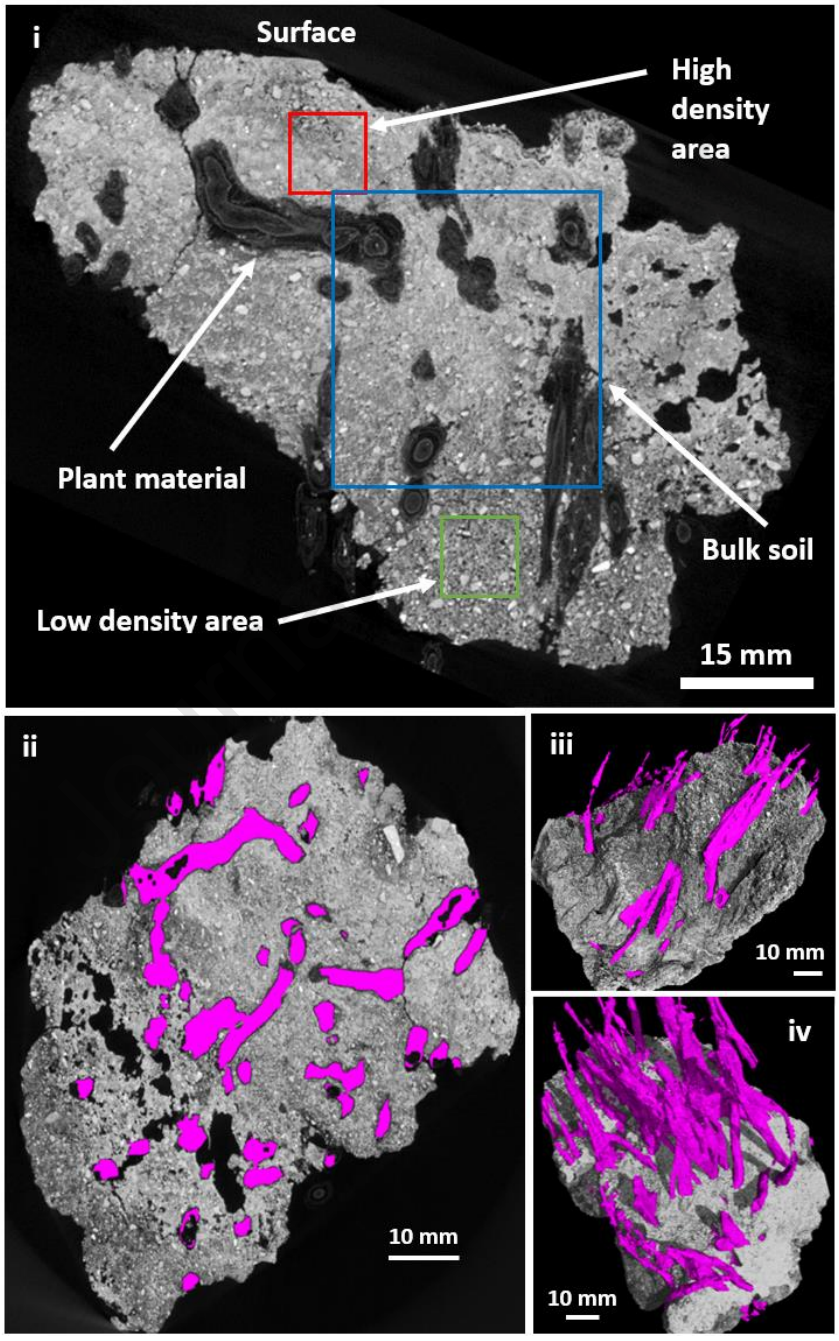

Fig. 3. Mineralization of a low concentration of ^{14}C-labelled glucose (10 µM) after addition to either (A) the phyllosphere soil, topsoil (0-20 cm) or subsoil (20-40 cm) associated with *D. spicata* plants or (B) in the corresponding areas of soil containing no plants. Values represent means ± SEM (n = 5).

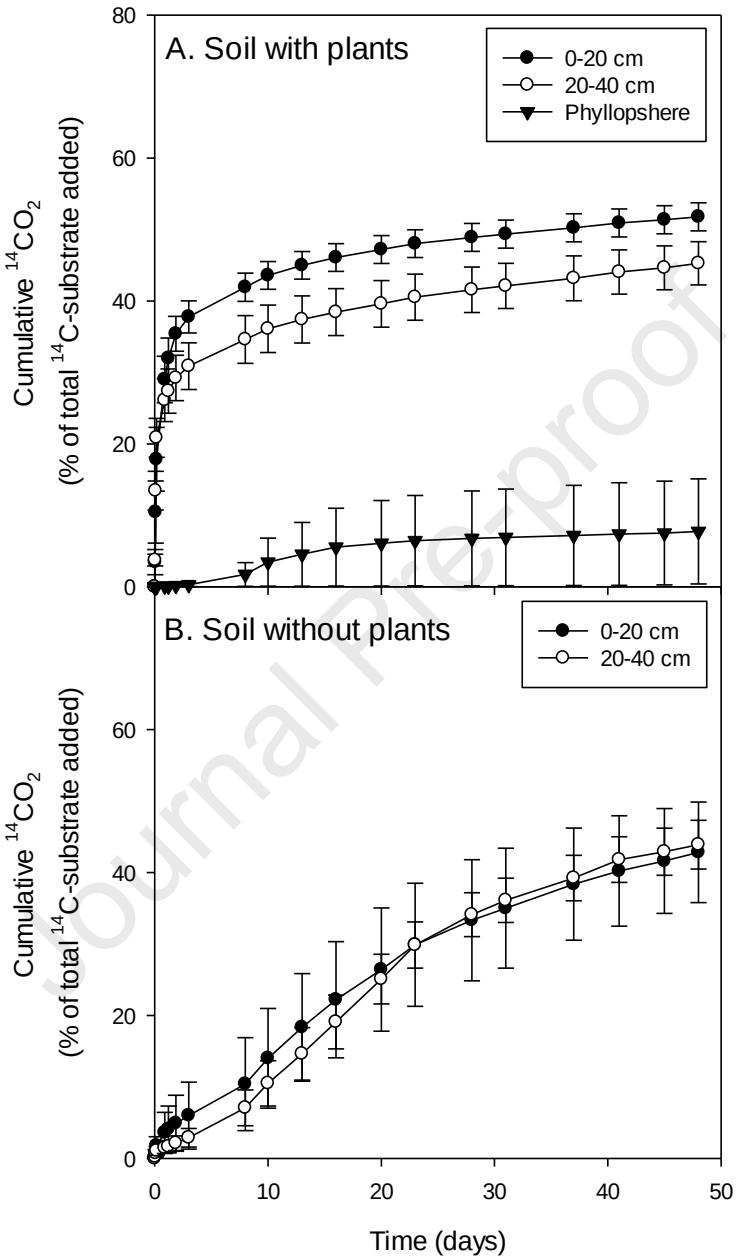

Fig. 4. Mineralization of a large concentration of ^{14}C-labelled glucose (10 mM) after addition to either (A) the phyllosphere, topsoil (0-20 cm) or subsoil (20-40 cm) associated with *D. spicata* plants or (B) in the corresponding areas of soil containing no plants. Values represent means ± SEM (n = 5).

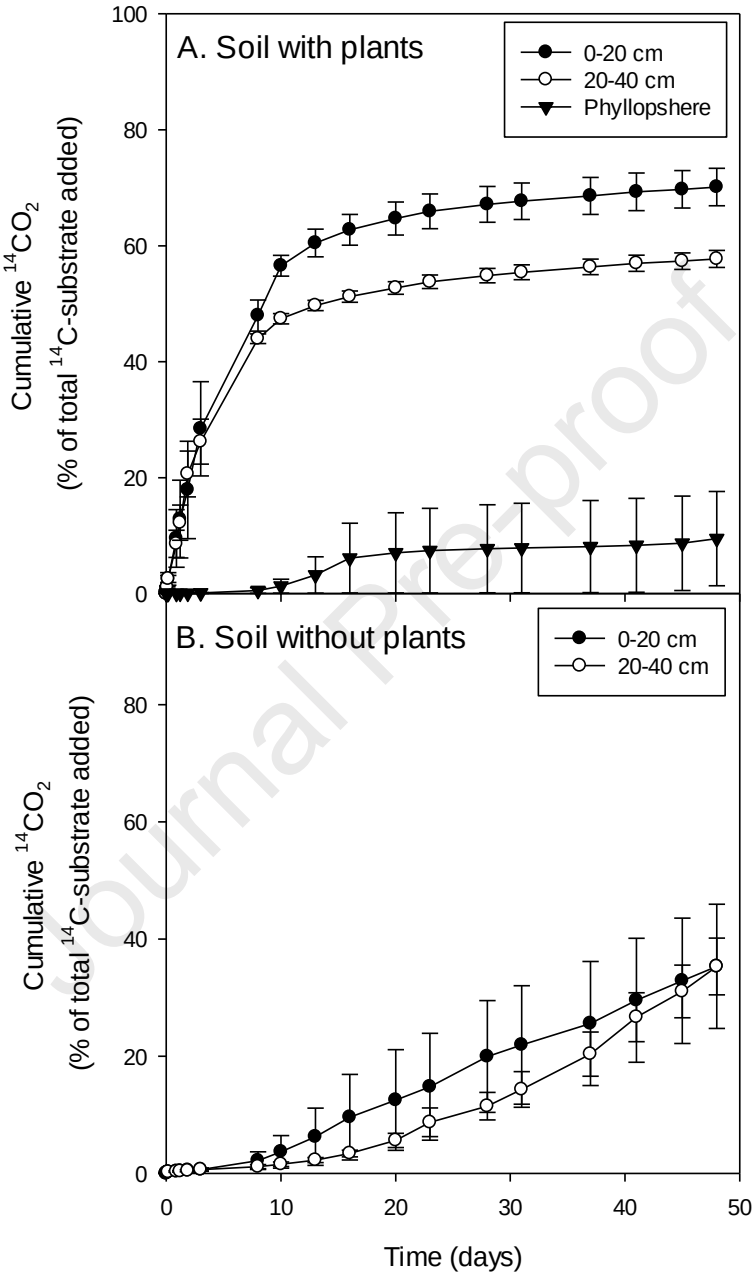

Fig. 5. Microbial carbon use efficiency (CUE) in either topsoil (0-20 cm) or subsoil (20-40 cm) in the presence or absence of plants (*D. spicata*) after the addition of a high (10 mM) or low (10 µM) dose of glucose to the soil. Values represent means ± SEM (n = 5). Different lowercase and uppercase letters represent significant differences between soils for the low and high glucose dose respectively ($P < 0.05$). NS and ** indicate differences of either $P > 0.05$ or $P < 0.01$ between the high and low glucose doses for individual soils.

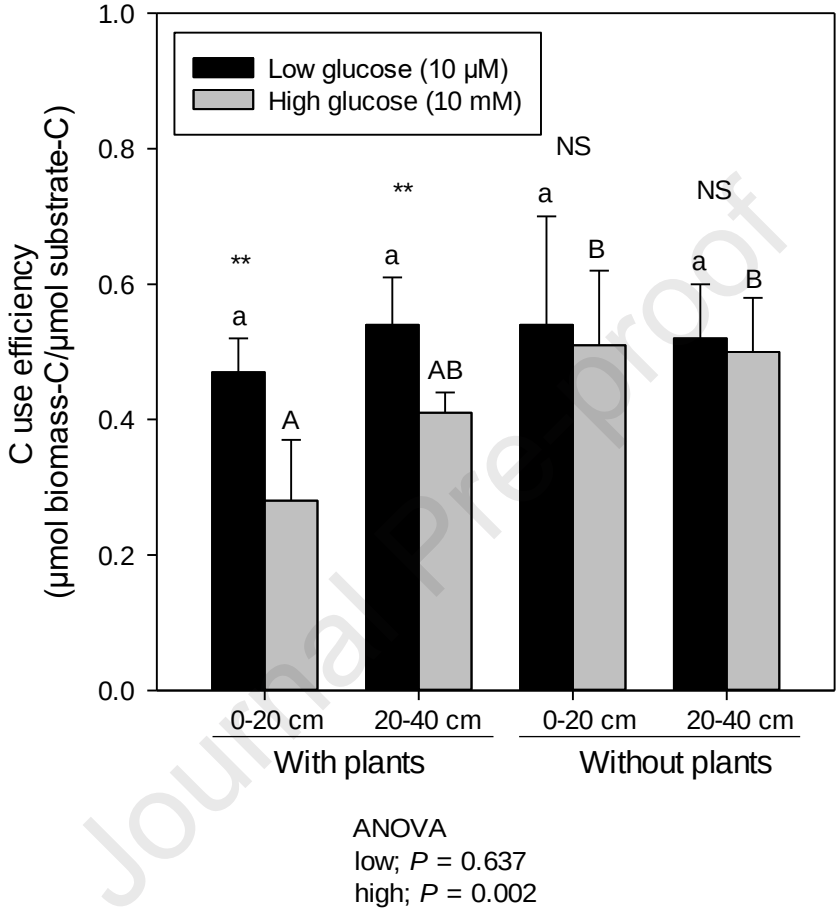

Fig. 6. Mineralization of ^{14}C-labelled plant litter (10 mg g^{-1}) after addition to either (A) the phyllosphere soil, underlying topsoil (0-20 cm) or subsoil (20-40 cm) associated with *D. spicata* plants or (B) in the corresponding areas of soil containing no plants. Values represent means ± SEM (n = 5).

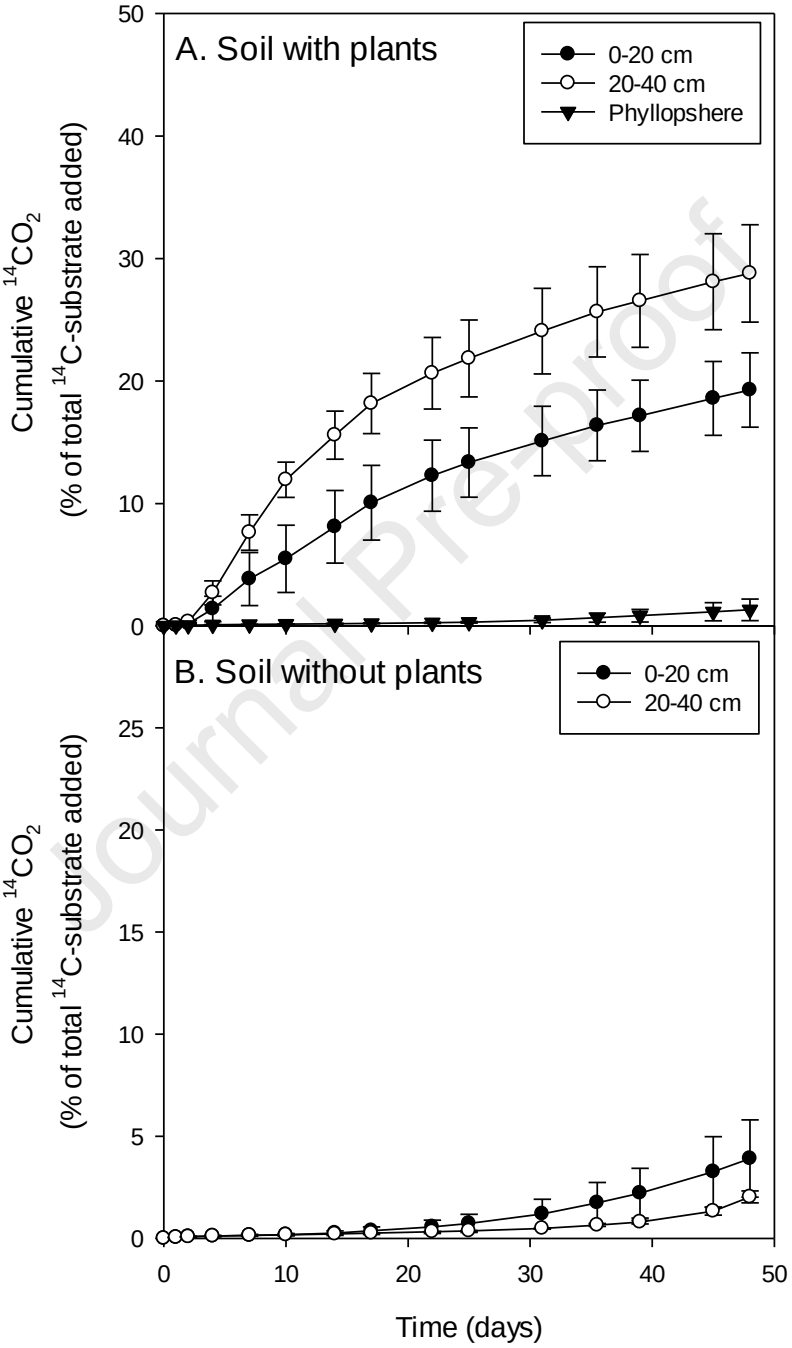

Fig. 7. Amount of $^{14}CO_2$, NH_4^+ and NH_3 produced after the addition of ^{14}C-labelled arginine to either the phyllosphere soil or underlying topsoil (0-20 cm) or subsoil (20-40 cm) associated with *D. spicata* plants or in the corresponding areas of soil containing no plants. Values represent means ± SEM (n = 5). Different letters represent significant differences between soils. The dotted line denotes the division between soils with and without plants.

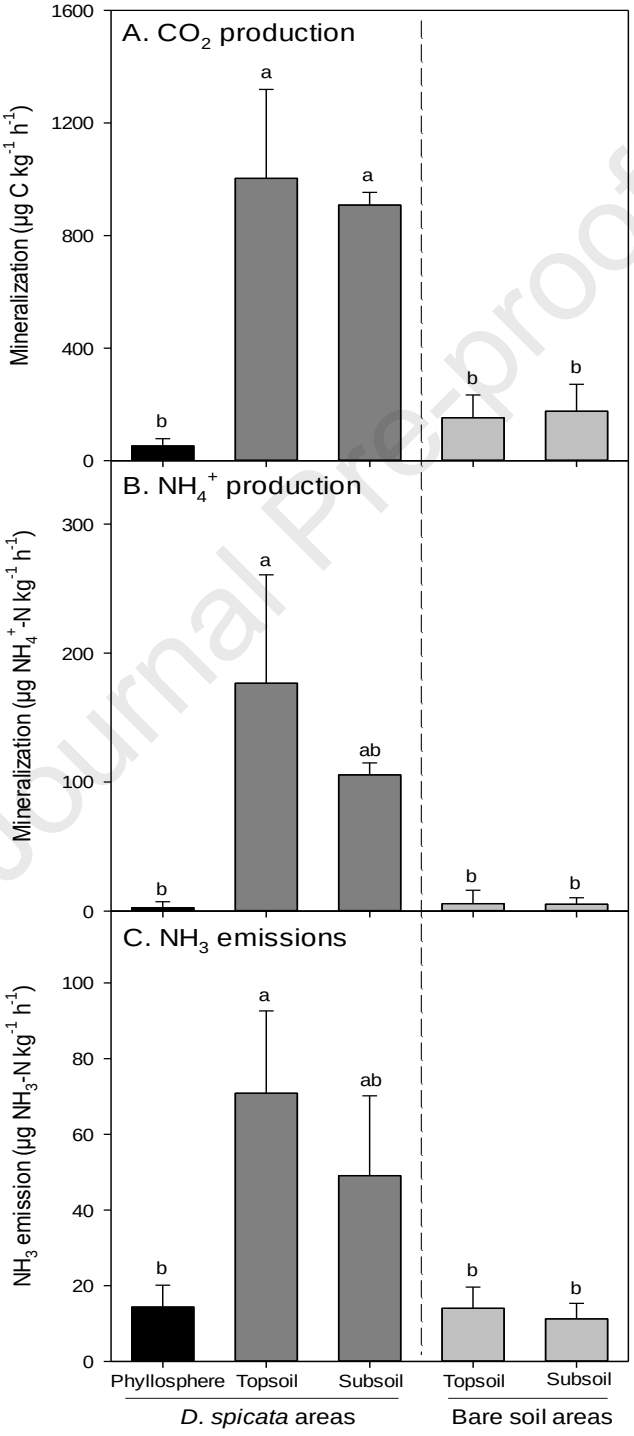

1230

Table 1. Chemical composition of the different tissues in *Distichlis spicata*.

Element	*Distichlis spicata*				*Adesmia atacamensis*	*Prosopis tamarugo*	*Atriplex atacamensis*	*P* value
	Fresh leaves	Senesced leaves	Stems	Roots	Fresh leaves	Fresh leaves	Fresh leaves	
Macronutrients (mg g^{-1})								
C	37.5 ±0.8^{c}	37.6 ±0.6^{c}	43.7 ±0.2^{a}	41.7 ±2.4^{ab}	44.2 ±1.3^{a}	44.5 ±0.5^{a}	36.4 ±0.6^{c}	***
N	1.11 ±0.07^{c}	0.50 ±0.02^{e}	0.67 ±0.03^{de}	0.93 ±0.05^{cd}	2.06 ±0.20^{b}	2.87 ±0.19^{a}	2.20 ±0.13^{b}	***
Na	37.6 ±7.0^{a}	20.3 ±4.0^{b}	10.5 ±1.9^{bc}	3.4 ±1.0^{c}	1.4 ±0.2^{c}	1.6 ±0.3^{c}	42.0 ±0.9^{a}	***
K	10.2 ±0.7^{b}	6.1 ± 0.6^{c}	6.0 ±0.7^{c}	5.0 ±0.7^{c}	3.9 ±0.4^{c}	7.1 ±1.9^{bc}	17.7 ±3.7^{a}	***
Mg	1.4 ±0.1^{a}	1.4 ±0.1^{a}	1.3 ±0.1^{a}	1.2 ±0.1^{a}	1.0 ±0.0^{b}	1.3 ±0.2^{a}	1.2 ±0.0^{a}	**
Ca	5.0 ±0.6^{b}	6.1 ±0.5^{b}	5.2 ±0.8^{b}	8.5 ±3.6^{b}	5.6 ±0.6^{b}	20.6 ±9.1^{a}	5.4 ±0.4^{b}	*
P	0.39 ±0.04^{b}	0.11 ±0.01^{c}	0.27 ±0.06^{bc}	0.34 ±0.05^{bc}	0.33 ±0.04^{bc}	0.47 ±0.21^{b}	0.93 ±0.27^{a}	***
S	2.72 ±0.25	4.60 ±0.16	4.35 ±0.56	5.44 ±2.12	3.37 ±0.34	6.34 ±3.87	2.95 ±0.22	NS
Cl	104.3 ±19.6^{a}	50.8 ±8.7^{b}	34.9 ±8.8^{bc}	11.6 ±0.9^{c}	11.8 ±0.8^{c}	11.2 ±1.6^{c}	58.6 ±0.3^{b}	***
Micronutrients (µg g^{-1})								
Fe	1200 ±184^{c}	2770 ±310^{a}	2225 ±449^{ab}	3103 ±1875^{c}	1311 ±170^{c}	1353 ±159^{bc}	490 ±23^{c}	***
Mn	135 ±10^{a}	119 ±9^{ab}	85 ±17^{abc}	72 ±28^{bc}	38 ±4^{c}	103 ±43^{abc}	131 ±19^{ab}	*
Ni	23 ±5^{cd}	25 ±2^{cd}	55 ±6^{a}	35 ±7^{bc}	50 ±3^{ab}	19 ±5^{cd}	13 ±4^{d}	***
Cu	38 ±4^{b}	62 ±4^{a}	20 ±10^{bcd}	15 ±2^{cd}	13 ±2^{cd}	34 ±14^{bc}	10 ±1^{d}	***
Zn	21 ±2^{bc}	37 ±4^{ab}	38 ±1^{a}	49 ±9^{a}	49 ±10^{abc}	46 ±12^{a}	17 ±2^{c}	*
Nutrient ratio								
C/N	34 ±3^{bc}	77 ±9^{a}	66 ±5^{a}	45 ±5^{b}	22 ±2^{cd}	16 ±1^{d}	17 ±2^{d}	***
Stable Isotopes (‰)								
$\delta^{13}C$	-15.3 ±0.2^{c}	-14.9 ±0.2^{bc}	-13.2 ±0.8^{a}	-14.1 ±0.2^{ab}	-25.3 ±0.8^{e}	-23.5 ±0.5^{d}	-15.0 ±0.4^{bc}	***
$\delta^{15}N$	21.7 ±7.7^{a}	13.6 ±0.5^{ab}	13.7 ±2.8^{ab}	12.0 ±2.8^{b}	5.8 ±1.1^{b}	11.9 ±0.1^{ab}	11.2 ±0.7^{b}	**

The nutrient composition of three other plants found at the site is provided for comparison. Values represent means ± SEM, $n = 5$ for *D. spicata* and $n = 3$ for the other species. Different letters indicate significant differences between groups at the $P < 0.05$ level. The *P* value ANOVA symbols *, ** and *** indicate significant differences at the $P < 0.05$, $P < 0.01$ and $P < 0.001$ level respectively, while NS indicates no significant difference ($P > 0.05$).

Table 2. Chemical composition of soils under *Distichlis spicata* and in adjacent areas with no plants present.

	Area with *D. spicata* plants			Area with no plants		*P* value
	Phyllosphere soil	Topsoil	Subsoil	Topsoil	Subsoil	
Sand (g kg^{-1})	539 ±25	432 ±51	435 ±99	385 ±105	298 ±58	NS
Silt (g kg^{-1})	211 ±18	316 ±23	349 ±79	422 ±76	420 ±46	NS
Clay (g kg^{-1})	174 ±17	220 ±28	203 ±23	151 ±30	230 ±23	NS
Soluble salts (g kg^{-1})[1]	77 $\pm15^{a}$	32 $\pm10^{bc}$	13 $\pm2^{c}$	43 $\pm8^{bc}$	52 $\pm16^{ab}$	**
$CaCO_3$ (g kg^{-1})	31 $\pm1^{ab}$	29 $\pm3^{b}$	32 $\pm5^{ab}$	49 $\pm4^{a}$	39 $\pm7^{ab}$	*
Moisture content (g kg^{-1})	29 $\pm2^{b}$	157 $\pm7^{a}$	184 $\pm21^{a}$	64 $\pm18^{b}$	67 $\pm17^{b}$	***
pH	7.73 $\pm0.20^{c}$	8.75 $\pm0.13^{ab}$	8.43 $\pm0.08^{b}$	8.70 $\pm0.16^{ab}$	9.01 $\pm0.03^{a}$	***
EC (mS cm^{-1})	45.9 $\pm7.5^{a}$	14.9 $\pm5.2^{bc}$	6.2 $\pm0.6^{c}$	21.9 $\pm5.2^{bc}$	24.8 $\pm7.8^{b}$	**
NH_4^+ (mg N kg^{-1})	1.81 $\pm0.59^{a}$	0.90 $\pm0.36^{ab}$	0.29 $\pm0.09^{b}$	0.76 $\pm0.22^{b}$	0.33 $\pm0.07^{b}$	*
NO_3^- (g N kg^{-1})	1.51 ±0.68	0.69 ±0.23	0.22 ±0.07	1.08 ±0.17	1.06 ±0.38	NS
Total phenols (mg kg^{-1})	282 $\pm49^{a}$	12.4 $\pm6.9^{b}$	1.44 $\pm0.41^{b}$	3.07 $\pm0.81^{b}$	1.71 $\pm0.36^{b}$	***
Extractable Na (g kg^{-1})	25.5 $\pm5.4^{a}$	10.4 $\pm3.7^{bc}$	3.4 $\pm0.7^{c}$	14.3 $\pm3.2^{abc}$	18.6 $\pm6.0^{ab}$	*
Extractable K (g kg^{-1})	1.26 $\pm0.26^{a}$	0.51 $\pm0.17^{b}$	0.25 $\pm0.03^{b}$	0.31 $\pm0.12^{b}$	0.34 $\pm0.06^{b}$	***
Extractable Ca (g kg^{-1})	2.67 $\pm0.30^{a}$	1.30 $\pm0.14^{b}$	1.07 $\pm0.04^{b}$	1.66 $\pm0.13^{b}$	1.35 $\pm0.11^{b}$	***
Olsen available-P (mg kg^{-1})	3.58 $\pm1.37^{b}$	0.91 $\pm0.42^{a}$	0.97 $\pm0.44^{a}$	1.78 $\pm0.35^{ab}$	1.87 $\pm0.53^{ab}$	*
Acetic acid available P (mg kg^{-1})	23.4 $\pm3.2^{b}$	44.4 $\pm6.4^{a}$	48.3 $\pm8.2^{a}$	15.2 $\pm2.7^{b}$	20.0 $\pm7.2^{b}$	**
Dissolved organic C (mg kg^{-1})	7086 $\pm1250^{a}$	85 $\pm43^{b}$	13 $\pm 5^{b}$	33 $\pm7^{b}$	20 $\pm4^{b}$	***
Total C (g kg^{-1})	1.07 $\pm0.11^{a}$	0.21 $\pm0.04^{b}$	0.16 $\pm0.03^{b}$	0.14 $\pm0.03^{b}$	0.18 $\pm0.03^{b}$	***
Total N (mg kg^{-1})	137 $\pm33^{a}$	64 $\pm6^{b}$	55 $\pm11^{b}$	101 $\pm14^{ab}$	97 $\pm15^{ab}$	*
Total soil C:N ratio	9.6 $\pm2.1^{a}$	3.3 $\pm0.7^{b}$	3.2 $\pm0.6^{b}$	1.4 $\pm0.2^{b}$	2.0 $\pm0.4^{b}$	***
Soil solution C:N ratio	7.51 $\pm2.56^{a}$	0.16 $\pm0.12^{b}$	0.07 $\pm0.04^{b}$	0.03 $\pm0.01^{b}$	0.03 $\pm0.01^{b}$	***
Ammonification rate (mg N kg^{-1} d^{-1})	6.41 $\pm2.12^{a}$	0.58 $\pm0.24^{b}$	0.36 $\pm0.07^{b}$	0.59 $\pm0.20^{b}$	0.34 $\pm0.09^{b}$	***

Values represent means ± SEM, $n = 5$. Different letters indicate significant differences between treatments ate the $P < 0.05$ level. Where appropriate, all values are expressed on a dry weight basis. The *P* value ANOVA symbols *, ** and *** indicate significant differences at the $P < 0.05$, $P < 0.01$ and $P < 0.001$ level respectively, while NS indicates no significant difference ($P > 0.05$).

Table 3. The carbon stocks of total soil organic C (SOC), recent (C_4-C) and older (C_3-C) in the soil compartment under *Distichlis spicata* or without plants (unvegetated).

Sample type	Soil ^{13}C (‰)	Amount of C_4-C (% of total)	SOC (g C kg^{-1})	C stocks (g C m^{-2})	Recent C_4-C (g C m^{-2})	Older C_3-C (g C m^{-2})
Phyllosphere	-13.93 ± 1.02	86 ± 7	10.8 ± 2.41	1941 ± 866	1674	267
Topsoil (vegetated)	-17.58 ± 1.60	60 ± 11	2.08 ± 0.92	748 ± 330	450	298
Subsoil (vegetated)	-18.05 ± 1.27	57 ± 9	1.60 ± 0.62	575 ± 223	327	249
Topsoil (unvegetated)	-24.78 ± 0.50	9 ± 4	1.36 ± 0.56	491 ± 201	43	448
Subsoil (unvegetated)	-23.67 ± 1.65	17 ±12	1.78 ± 0.56	642 ± 202	107	536

Values represent means ± SD or means only (n = 5). The soil bulk density was assumed to be 1.8 g cm^{-3}. Sampled soil depth interval were topsoil (0-20 cm) and subsoil (20-40 cm), except the phyllosphere soil for which only 10 cm was sampled from the plant column. The ^{13}C endmember plant C_4 plant (100%) were set to -12‰ and C_3 (100%) set to -26‰.

Table 4. Microbial biomass and the relative abundance of different microbial groups within the topsoil, subsoil and phyllosphere soil of *Distichlis spicata* in comparison to areas of bare ground where no plants are present.

	Area with *Distichlis spicata*			Area with no plants		*P* value
	Phyllosphere soil	Topsoil	Subsoil	Topsoil	Subsoil	
Microbial biomass (nmol g^{-1})	2.33 ± 1.03^{b}	10.7 ± 3.60^{a}	12.3 ± 3.44^{a}	1.37 ± 0.41^{b}	0.62 ± 0.29^{b}	**
Gram- bacteria (nmol g^{-1})	0.74 ± 0.38^{bc}	2.48 ± 1.20^{a}	3.34 ± 1.08^{ab}	0.49 ± 0.16^{bc}	0.16 ± 0.11^{c}	*
Gram+ bacteria (nmol g^{-1})	1.38 ± 0.69^{b}	7.05 ± 2.19^{a}	8.03 ± 2.24^{a}	0.80 ± 0.23^{b}	0.43 ± 0.16^{b}	**
Putative AMF (nmol g^{-1})	<0.05	0.15 ± 0.01^{a}	0.19 ± 0.02^{a}	<0.05	<0.05	NS
Fungi (nmol g^{-1})	0.21 ± 0.08^{a}	0.48 ± 0.12^{a}	0.24 ± 0.06^{a}	<0.05	<0.05	NS
Actinomycetes (nmol g^{-1})	<0.05	0.52 ± 0.19^{a}	0.69 ± 0.19^{a}	0.08 ± 0.05^{b}	0.03 ± 0.02^{b}	**

Values represent means ± SEM, $n = 5$. Different superscript letters indicate significant differences between treatments ate the $P < 0.05$ level. The *P* value ANOVA symbols *, ** and *** indicate significant differences at the $P < 0.05$, $P < 0.01$ and $P < 0.001$ level respectively, while NS indicates no significant difference ($P > 0.05$).

Supplementary on-line information

Life at the extreme: Plant-driven microbial hotspots of nutrient cycling in the hyper-arid core of the Atacama Desert

Davey L. Jones[a,b,*], Bárbara Fuentes[c], Franko Arenas-Díaz[d], Francisco Remonsellez[e], Rutger van Hall[f] , Brian S. Atkinson[g], Sacha J. Mooney[g], Roland Bol[h,a]

[a] *SoilsWales, School of Natural Sciences, Bangor University, Gwynedd, LL57 2UW, UK*

[b] *SoilsWest, Centre for Sustainable Farming Systems, Food Futures Institute, Murdoch University, Murdoch, WA 6150, Australia*

[c] *Departamento de Ingeniería Química, Universidad Católica del Norte, Antofagasta, Chile*

[d] *Programa de Doctorado en Ciencias mención Geología, Departamento de Cs. Geológicas, Universidad Católica del Norte, Antofagasta, Chile*

[e] *Centro de Investigación Tecnológica del Agua en el Desierto-CEITSAZA, Universidad Católica del Norte, Antofagasta, Chile*

[f] *Institute for Biodiversity and Ecosystem Dynamics, University of Amsterdam, Science Park 904, 1090 GE, Amsterdam, The Netherlands*

[g] *Agricultural and Environmental Sciences, School of Biosciences, University of Nottingham, Nottingham, LE12 5RD, UK*

[h] *Institute of Bio- and Geosciences, Agrosphere Institute (IBG-3), Forschungszentrum Jülich, 52425 Jülich, Germany*

Fig. S1. Geographical location of the study site in the Atacama Desert, Chile. The red boxes denotes the location of the study site.

Fig. S2. Aerial photograph of the study site (red square). The plants are located in the darker areas. The site is flat. The ephemeral braided river (Quebrada del Profeta) in which the study site is located can be seen as the lighter area relative to the surrounding desert.

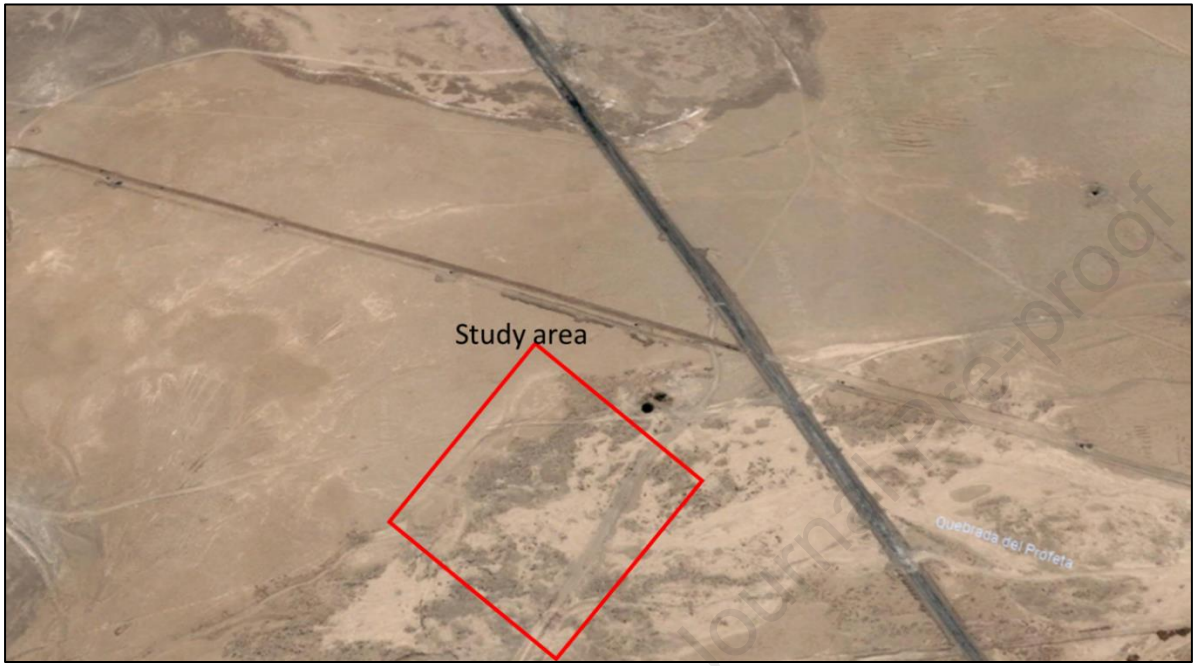

Fig. S3. Photograph of the study site showing the bare soil and isolated columnar shaped vegetation mounds.

Fig. S4. Photographs showing young (left) and mature (right) plants of *Distichlis spicata.* Only the larger mature plants were sampled in this study.

Fig. S5. Soil profile at the study site within the bare soil area. The depth of soil shown is 30 cm. The plant columns can be seen in the background. Although the soil contains high amounts of nitrate, it does not have enough to classify it as possessing a nitric diagnostic horizon (> 12 cmol l^{-1} in a 1:5 (w/v) soil/water extract; Finstad et al., 2014). The soil has a hyper-arid soil moisture regime with rainfall averages which are incapable of removing soluble salts from the upper 150 cm over long-time scales, therefore allowing the formation of indurated horizons.

Fig. S6. Field team investigating the soil under the mature *Distichlis spicata* plants. In order to minimize environmental damage, a hole was excavated to the side of the plant and then samples taken laterally underneath the plant.

Fig. S7. Schematic representation of the sampling points. Intact soil samples for X-ray CT analysis were taken from the cemented/indurated 0-5 cm soil layer. For soil microbial activity and other physical and chemical analysis, soil samples were taken from the 5-15 cm and 20-40 cm layers. For the soil trapped in the phyllosphere, soil was taken 60 cm above ground level. The latter included a 10 cm layer of soil from the plant column.

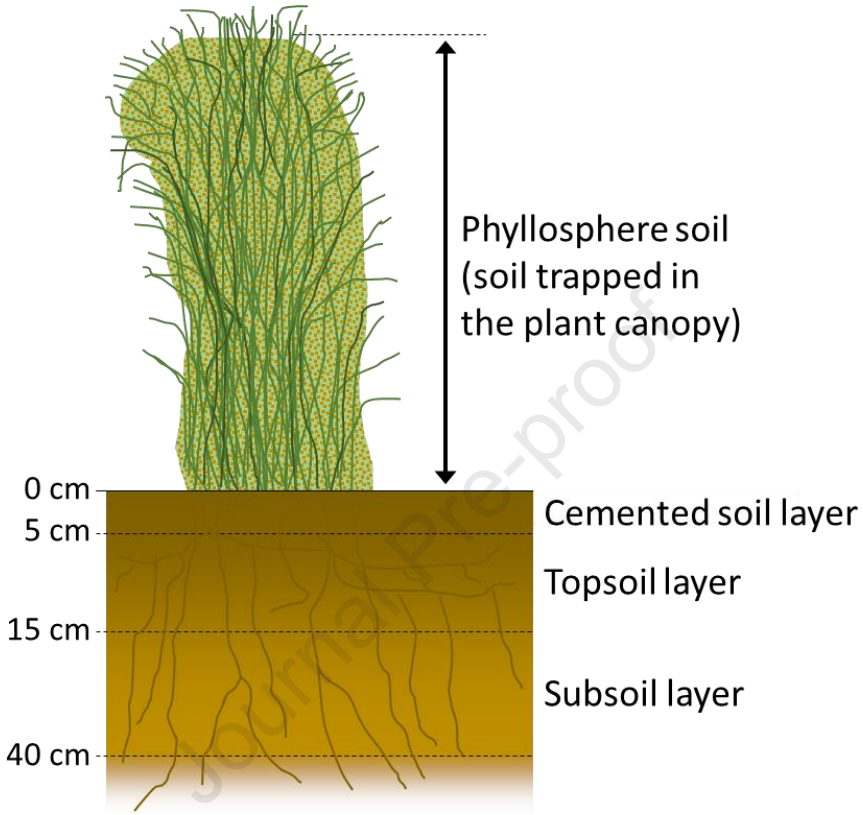

Fig. S8. Length of day and night for the field site.

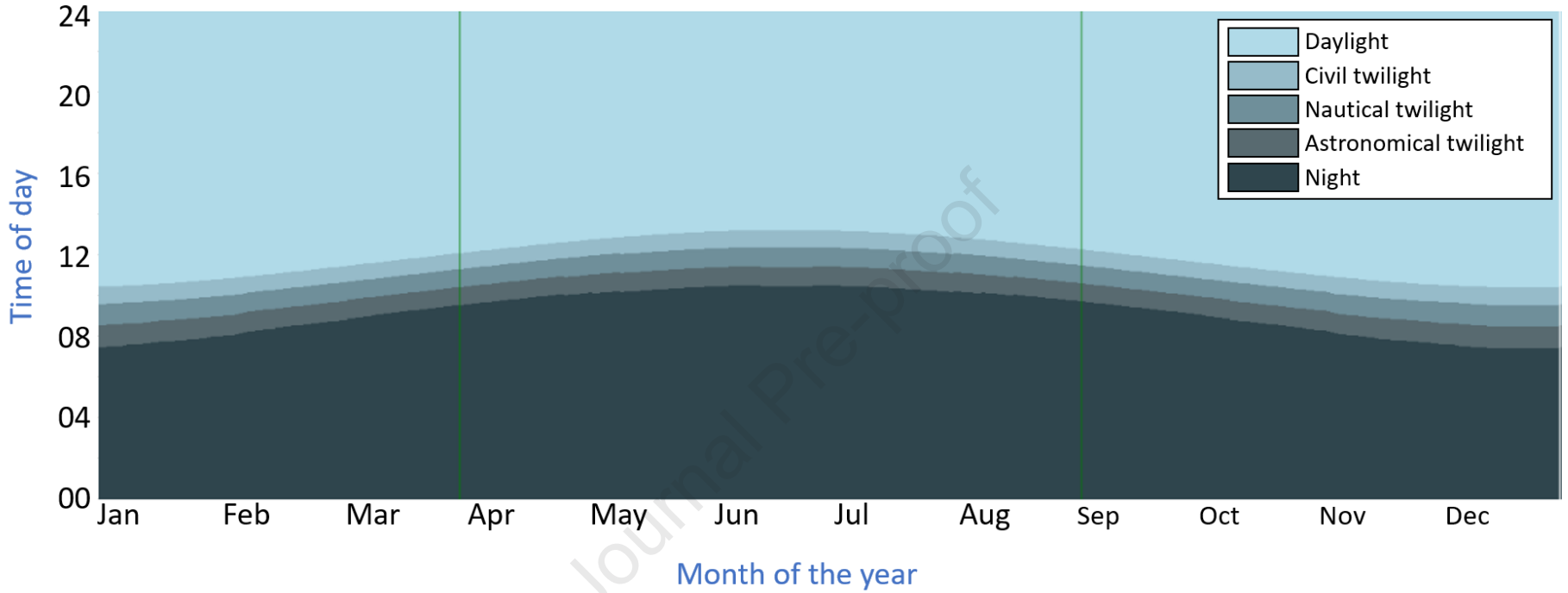

Fig S9. Box plots showing the distribution in temperature and relative humidity in the plant above-ground canopy, surface soil (1 cm) and subsurface soil (10 cm) at the field site. Values represent hourly samples taken over a 6-month period (n = 3893). The dotted lines represent the mean values and the solid line represents the median.

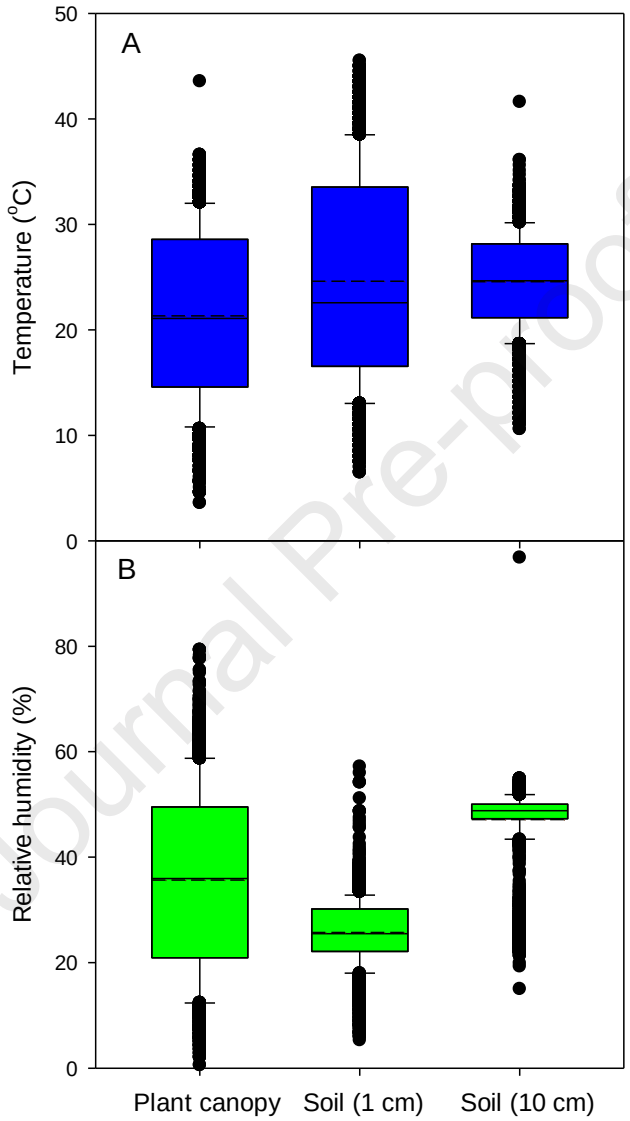

Fig. S9. Photographs showing (a) *Distichlis spicata* growing in columns in the Atacama Desert, (b) the abundance of salt crystals on the leaves, (c) the presence of organic matter in the phyllosphere soil, (d) X-ray imaging showing the passage of roots through the cemented soil.

a)

b)

c)

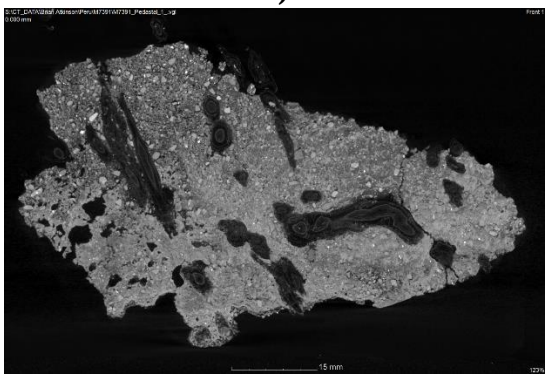

d)

Fig. S10. The $\delta^{13}C$ and $\delta^{15}N$ ratio of leaves from the four main plants found at the field site in the Atacama Desert. It should be stated that only *D. spicata* was found in high abundance with the other species only found very occasionally (i.e. < 0.001% of the plants in the area). Symbols reflect individual replicate plants found within the study area.

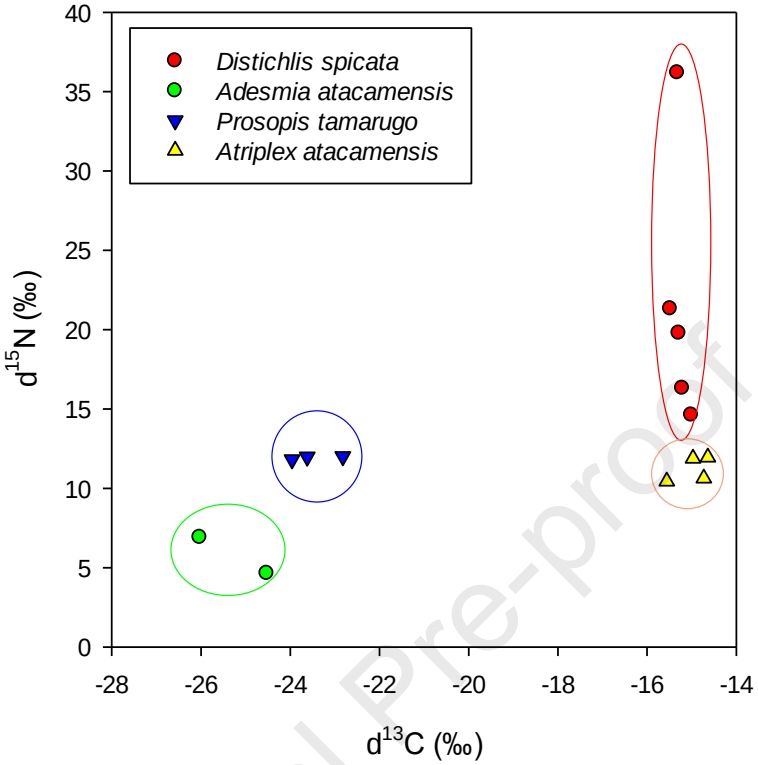

Fig. S11. $\delta^{13}C$ and $\delta^{15}N$ ratio of the different plant tissues within *Distichlis spicata* found at the field site in the Atacama Desert. Symbols reflect individual replicate plants found within the study area (n = 5).

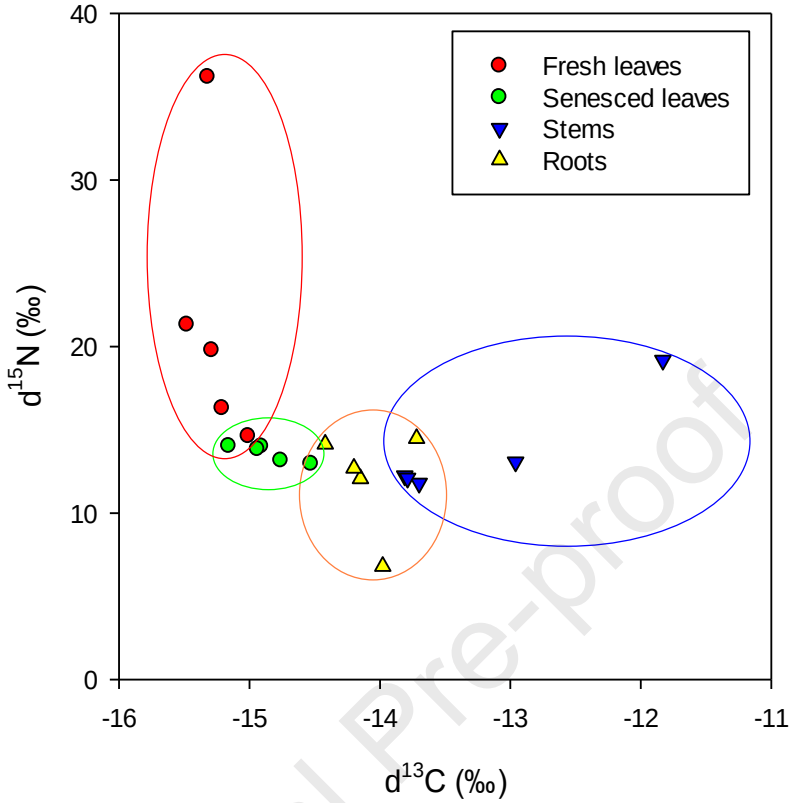

Fig. S12. The $\delta^{13}C$ and $\delta^{15}N$ of vegetated and unvegetated soil and that trapped in the phyllosphere of *D. spicata*. Soil ^{15}N values are provided on the y-axis and the ^{13}C values on the x-axis. Yellow – Soil with no plants; Green – Soil with *D. spicata* plants; Blue – soil trapped in the phyllosphere of the *D. spicata* plants. Arrows on the x-axis represent the percentage recent (C_4-C) of the soil C.

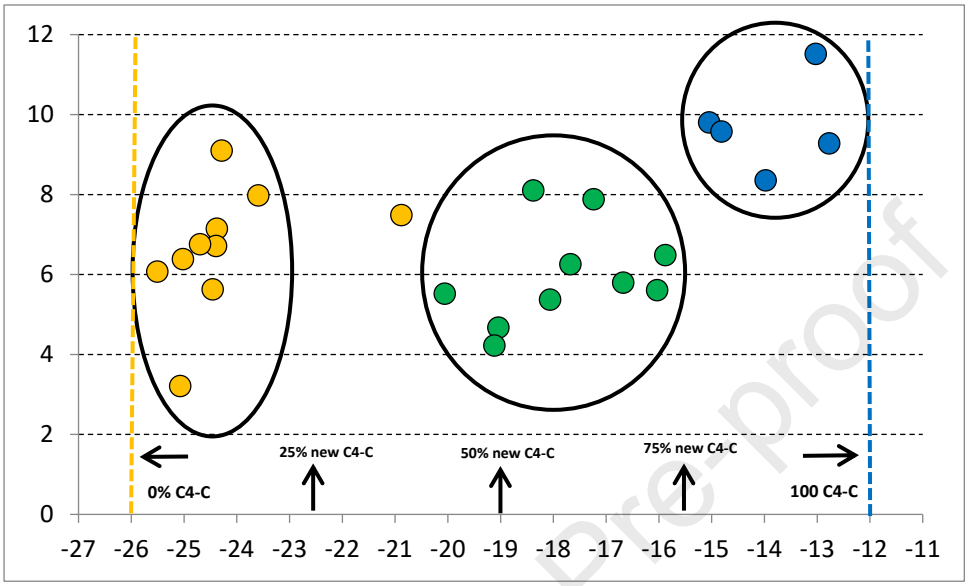

Fig. S10. A) Image analysis of pedestal showing the bulk soil differences (areas marked in white on the bulk grey scale image are the image mask where plant material was excluded from the pore analysis) in pore frequency from grey scale image to binary analysis and the distribution of pore sizes in comparison across the pedestal. B) Pore size distributions for low- and high-density areas (note the scale difference in ROI for sampling areas due to the need to avoid plant material). The high-density (cemented) areas are directly at the soil surface while the low-density areas underlie this highly cemented region.

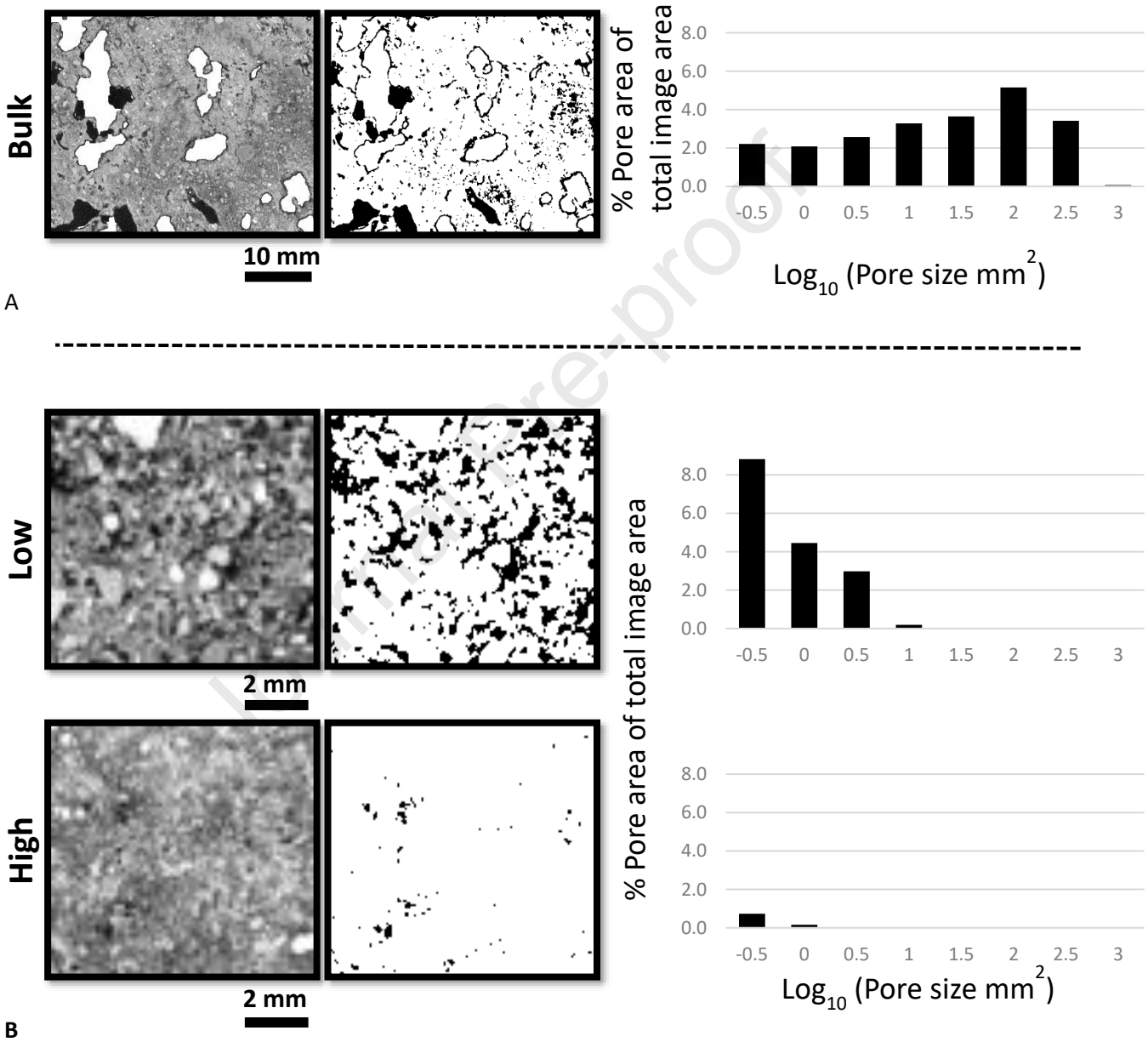

Fig. S14. Relationship between electrical conductivity and soluble salt content (Na + K + Ca) across all the soil samples analysed in the study. The line represents a fit of a linear regression equation to the experimental data.

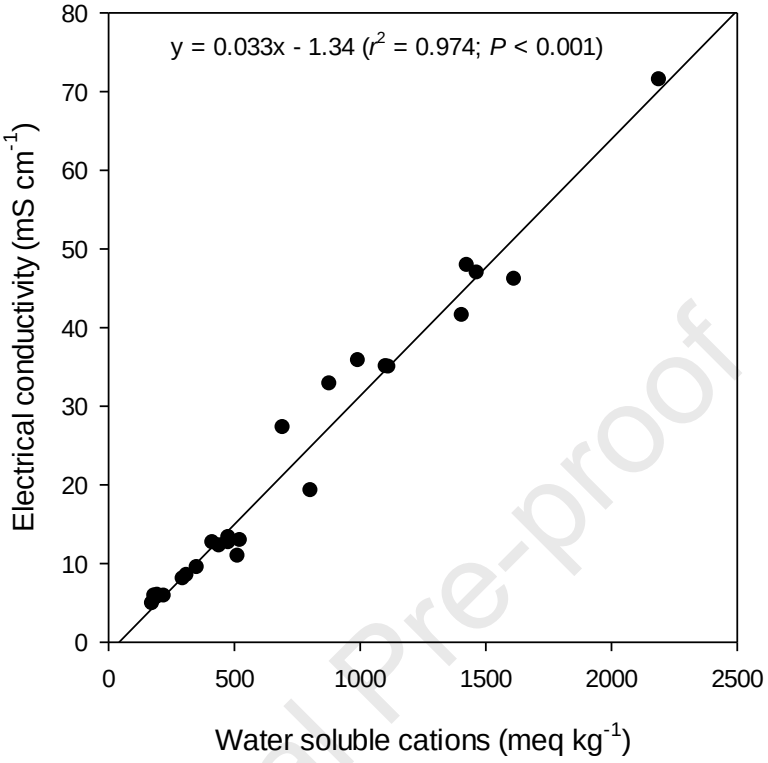

Fig. S15. Relationship between the rate of arginine mineralization to CO_2 and NH_4^+ across all the soil samples analysed in the study. The line represents a fit of a linear regression equation to the experimental data.

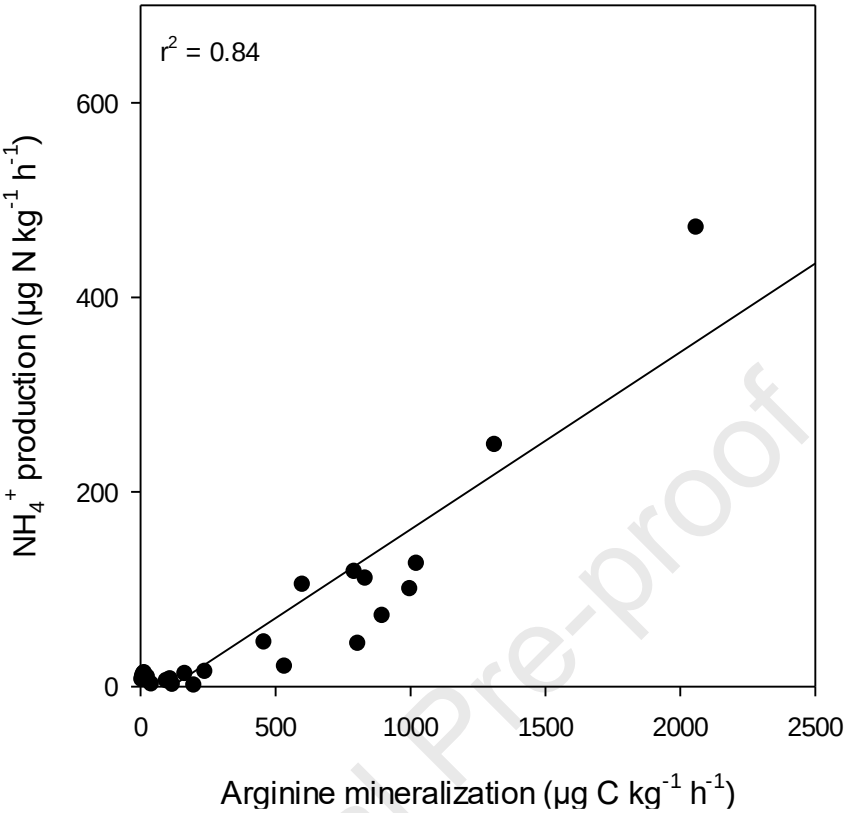

Fig. S16. Relationship between the rate of arginine mineralization and the rate of NH_3 release across all the soil samples analysed in the study. The line represents a fit of a linear regression equation to the experimental data.

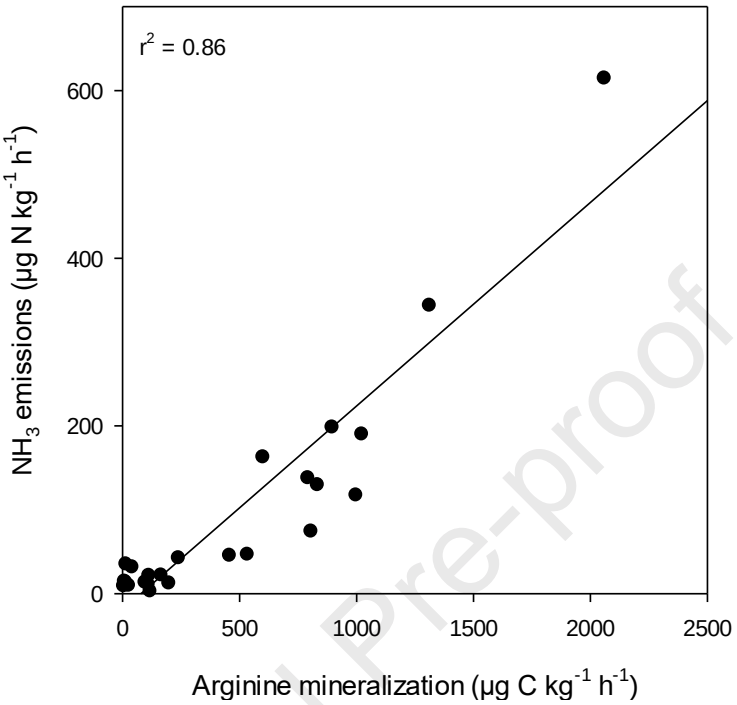

Fig. S17. Phosphorus sorption isotherms showing the relationship between P in solution and P held on the solid phase in the plant above-ground canopy soil (phyllosphere soil), soils under *D. spicata* (topsoil and subsoil) and in the corresponding unvegetated soils at the field site. Values represent means ± SEM (n = 5). The lines represent fits to the experimental data.

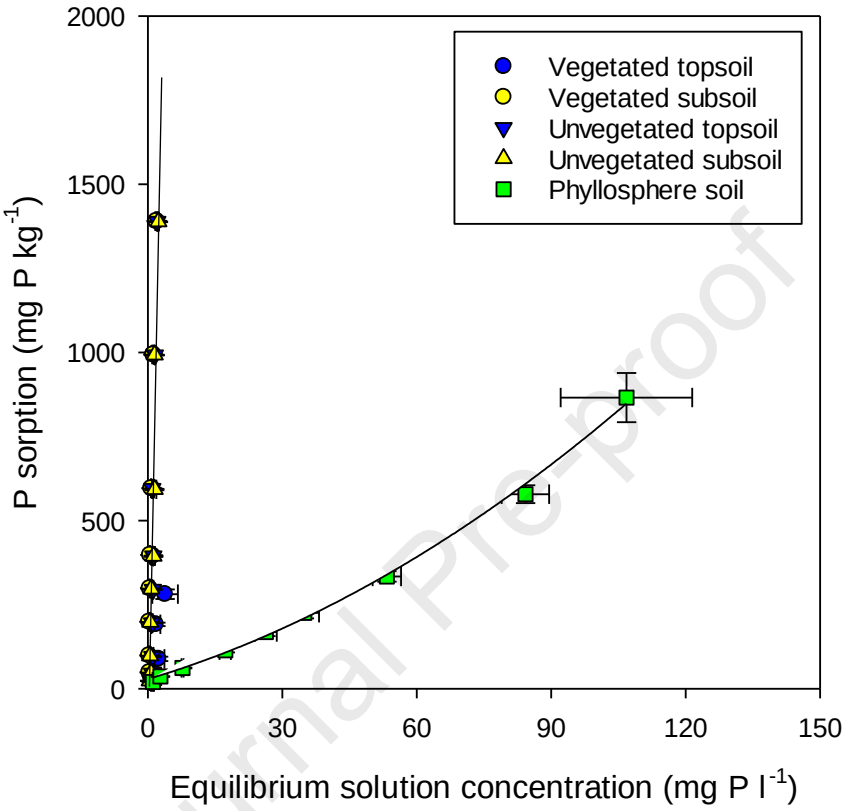

To calculate the P buffer power (B_p) of the soil (Barber, 1995) the following calculations were performed as follows where

$$B_p = C_{tot}/C_{sol} \quad \text{(Eqn. 1)}$$

and where

$$C_{tot} = (C_{ads} \times BD) + (C_{sol} \times \Theta) \quad \text{(Eqn. 2)}$$

C_{tot} is defined as the total amount of P in the soil, C_{ads} is the amount of P sorbed to the solid phase, BD is soil bulk density (assumed here to be 1.3. g cm^{-3}), C_{sol} is the equilibrium solution concentration and Θ is the soil volumetric water content.

Fig. S18. Photographs of the top of the *D. spicata* canopy (upper left), a new *D. spicata* plant establishing (upper right) and a *D. spicata* column.

Fig. S19. Drone shot of the study site. The dark patches represent areas of *D. spicata* growth.

Table S1. GPS locations of the individual *D. spicata* plants sampled and the control areas.

Location	**Latitude and longitude co-**ordinates	
Plant 1	-24.04761200000000	-69.82636028180270
Plant 2	-24.04705000000000	-69.82674023809560
Plant 3	-24.04695100000000	-69.82659208753660
Plant 4	-24.04662600000000	-69.82666868129420
Plant 5	-24.04800400000000	-69.82721841642080
Control 1	-24.04770200000000	-69.82547054907910
Control 2	-24.04678800000000	-69.82680740188950
Control 3	-24.04678800000000	-69.82680740188950
Control 4	-24.04666100000000	-69.82677708969920
Control 5	-24.04770600000000	-69.82718700459070

Table S2. Minimum, maximum and mean average temperatures and relative humidities just prior to dawn (06.00-07.00 h) and early afternoon (14.00-15.00 h). See Figure S8 for information on day lengths during the study period (October-March).

	Temperature (°C)			Relative humidity (%)		
	Plant canopy	Surface soil	Subsurface soil	Plant canopy	Surface soil	Subsurface soil
			Time of day: 06.00-07.00 h			
Minimum	3.6	6.5	11.1	20.9	13.8	22.0
Mean	11.9	12.8	20.0	51.1	29.8	47.2
Maximum	21.6	22.6	26.2	77.7	40.6	54.9
			Time of day: 14.00-15.00 h			
Minimum	25.6	33.5	23.2	3.6	7.7	19.3
Mean	32.0	39.6	27.2	15.6	21.8	46.7
Maximum	36.6	45.0	36.1	28.5	32.2	53.7

Table S3. Average pore morphology characteristics (Pore size, porosity and coefficient of uniformity, PSD_{cu}) of the bulk soil at the cemented soil surface (0-5 cm depth) at the base of the plant columns with focus on the comparison of the high-density and low-density areas (see Figure 2 for further details).

	Bulk soil	High density soil	Low density soil
Average pore size (mm^2)	0.97	0.13	0.20
Porosity (%)	22.4	0.89	16.5
PSD_{cu}	90.6	6.0	8.1

Table S4. Phospholipid-derived fatty acids (PLFAs) considered in the study to establish the different taxonomic groups within the soil samples.

Biomarker	Taxonomic group	References
14:0 iso, 15:0 iso, 15:0 anteiso, 15:1 iso w6c, 16:0 iso, 17:0 iso, 17:0 anteiso, 17:1 iso w9c,	Prokaryotes: Gram+ bacteria	Ratledge and Wilkinson (1988), Kieft et al. (1994), Paul and Clark (1996), Zelles (1999), Olsson et al. (1999), Bartelt-Ryser et al. (2005)
16:1w7c, 16:1w9c, 17:1w8c, 17:0 cyclo w7c, 18:1w5c, 18:1w7c, 18:1w9c, 19:0 cyclo w7c	Prokaryotes: Gram− bacteria	Bedard and Knowles (1989), Bossio and Scow (1998), Bowman et al. (1991, 1993), Kieft et al. (1994), Paul and Clark (1996), Zelles (1999)
16:0 10 methyl, 18:0 10 methyl, 10 methyl 19:1 w7c	Prokaryotes: actinomycetes, Gram+ bacteria	Zelles (1999)
15:0 dma	Prokaryotes: Anaerobic bacteria	
20:4w6	Eukaryotes: protozoa	Paul and Clark (1996)
18:2w6c	Eukaryotes: fungi	Paul and Clark (1996)
16:1w5c	Eukaryotes: putative arbuscular mycorrhiza, fungi	Olsson et al. (1999)
14:0, 15:0, 16:0, 17:0, 18:0	Not assigned to a taxonomic group	Ratledge and Wilkinson (1988), Niklaus et al. (2003)

Glucose turnover in soil

Modelling glucose turnover (10 µM) in the vegetated soil using the double exponential kinetics decay model of Glanville et al. (2016). The reader is advised to read the associated paper to get a full understanding of the C pools being modelled. The equation used to describe the loss of substrate from the soil as $^{14}CO_2$ is as follows:

$$\text{Loss of } {}^{14}CO_2 = (\textit{Catabolic}\text{-C} \times \exp^{-k_1 t}) + (\textit{Anabolic}\text{-C} \times \exp^{-k_2 t}) \quad \text{(Eqn. 3)}$$

Where *Catabolic*-C describes the amount of C allocated to energy and respiration, *Anabolic*-C represents the amount of C allocated to building and repairing cell biomass and where k_1 and k_2 are the rate constants describing the turnover of the catabolic and anabolic C pools respectively. Finally, t is time. The half-life of the two pools can be calculated as follow:

$$\text{Half-life of the Catabolic-C pool} = \ln(2)/k_1 \quad \text{(Eqn. 4)}$$

or

$$\text{Half-life of the anabolic-C pool} = \ln(2)/k_2 \quad \text{(Eqn. 5)}$$

The model was fitted in the programme SigmaPlot v14.5 using a least squares iteration routine (Glanville et al., 2016). The fit of the experimental data to the model was good (Topsoil $r^2 = 0.981$, Subsoil $r^2 = 0.979$). The model could only be fitted to the low concentration of glucose in the vegetated soil. In a perfectly fitted models the sum of the two pools is 100%. The deviation from this reflects the small error in the fitted model.

Table S5. Modelled kinetic parameters describing the turnover of a low concentration of glucose (10 uM) in the vegetated topsoil and subsoil from the hyperarid core of the Atacama Desert. SEM indicated standard error.

	Topsoil		Subsoil	
	Mean	SEM	Mean	SEM
Catabolic-C (%)	35.47	1.95	31.01	2.07
k_1 (days)	1.45	0.26	6.89	1.17
Anabolic-C (%)	60.57	1.48	70.20	0.91
k_2 (days)	0.0055	0.0009	0.006	0.0006
Half-life of Catabolic-C pool (days)	0.48		0.10	
Half-life of Anabolic-C pool (days)	126		116	

References

Barber, S.A., 1995. Soil Nutrient Bioavailability: A Mechanistic Approach, 2nd Edition, Wiley, New York. ISBN: 978-0-471-58747-7

Bartelt-Ryser, J., Joshi, J., Schmid, B., Brandl, H., Balser, T., 2005. Soil feedbacks of plant diversity on soil microbial communities and subsequent plant growth. Perspectives in Plant Ecology, Evolution and Systematics 7, 27–49.

Bedard, C., Knowles, R., 1989. Physiology, biochemistry, and specific inhibitors of CH_4, NH_4^+, and CO oxidation by methanotrophs and nitrifiers. Microbiology Reviews 53, 68−84.

Bossio, D.A., Scow, K.M., 1998. Impacts of carbon and flooding on soil microbial communities: phospholipid fatty acid profiles and substrate utilization patterns. Microbial Ecology 35, 265–278.

Bowman, J.P., Skerratt, J.H., Nichols, P.D., Sly, L.I., 1991. Phospholipid fatty-acid and lipopolysaccharide fatty-acid signature lipids in methane-utilizing bacteria. FEMS Microbiology Ecology 85, 15−22.

Bowman, J.P., Sly, L.I., Nichols, P.D., Hayward, A.C., 1993. Revised taxonomy of the methanotrophs – description of methylobacter gen-nov, emendation of methylococcus, validation of methylosinus and methylocystis species, and a proposal that the family methylococcaceae includes only the group-I methanotrophs. International Journal of Systematic Bacteriology 43, 735−753.

Finstad, K., Pfeiffer, M., Amundson, R., 2014. Hyper-arid soils and the soil taxonomy. Soil Science Society of America Journal 78, 1845-1851.

Glanville, H.C., Hill, P.W., Schnepf, A., Oburger, E., Jones, D.L., 2016. Combined use of empirical data and mathematical modelling to better estimate the microbial turnover of

isotopically labelled carbon substrates in soil. Soil Biology and Biochemistry. 94, 154-168. https://doi.org/10.1016/j.soilbio.2015.11.016

Kieft, T.L., Ringelberg, D.B., White, D.C., 1994. Changes in ester linked phospholipid fatty acid profiles of subsurface bacteria during starvation and desiccation in a porous medium. Applied and Environmental Microbiology 60, 3292–3299.

Niklaus, P.A., Alphei, J., Ebersberger, D., Kampichler, D., Kandeler, E., Tscherko, D., 2003. Six years of in situ CO_2 enrichment evoke changes in soil structure and soil biota of nutrient-poor grassland. Global Change Biology 9, 585–600.

Olsson, P.A., Thingstrup, I., Jakobsen, I., Baath, F., 1999. Estimation of the biomass of arbuscular mycorrhizal fungi in a linseed field. Soil Biology & Biochemistry 31, 1879–1887.

Paul, E.A., Clark, F.E., 1996. Soil Microbiology and Biochemistry. Academic Press, San Diego.

Ratledge, C., Wilkinson, S.G., 1988. Microbial Lipids. Academic Press, London.

Zelles, L., 1999. Fatty acids patterns of phospholipids and lipopolysaccharides in the characterization of microbial communities in soil: a review. Biology & Fertility of Soils 29, 111–129.

Movie S1.

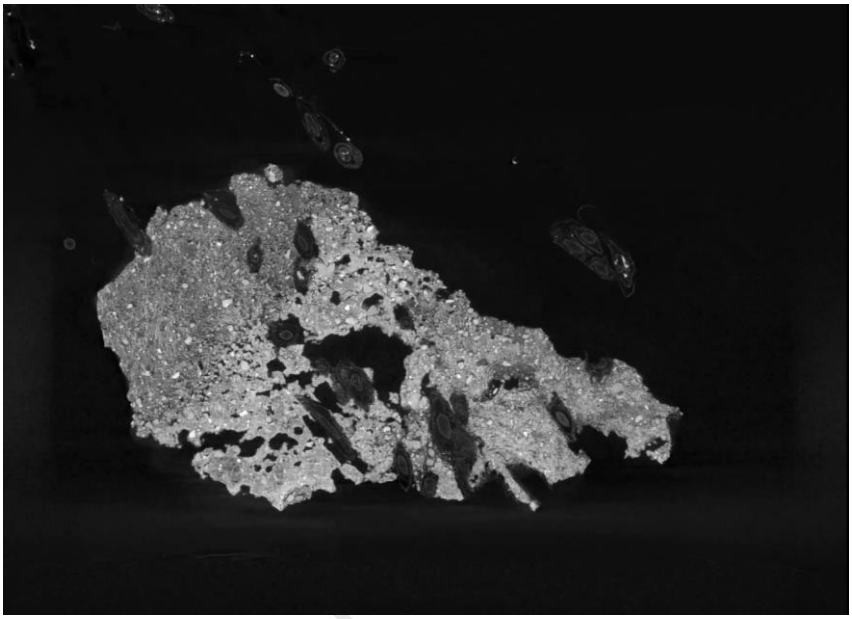

Movie S2.

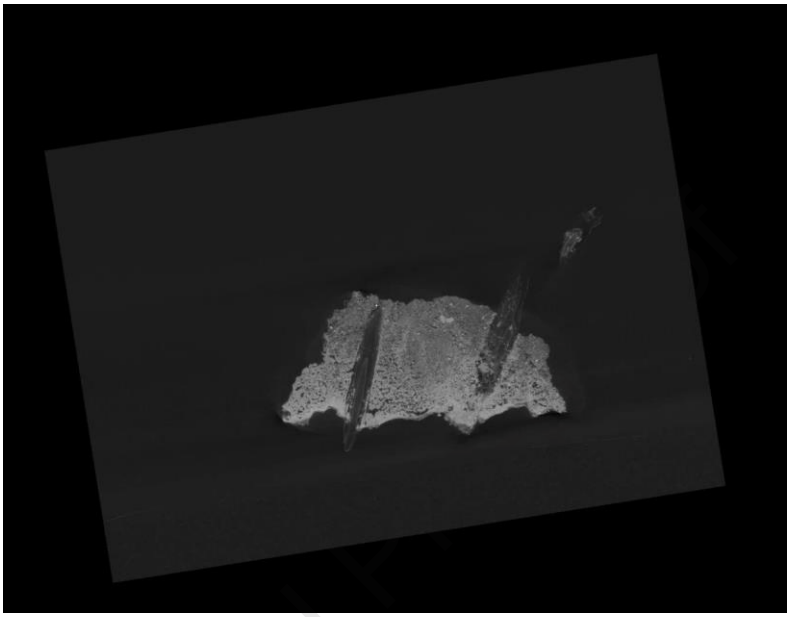

HIGHLIGHTS

- The hyperarid core of the Atacama Desert is one of the most extreme places on Earth
- Halophytic C4 *Distichlis spicata* is one of the few plants capable of survival
- *D. spicata* reengineers the soil to create below-ground biological hotspots
- *D. spicata* promotes microbial activity and more efficient biogeochemical cycling
- Soil biological activity is limited by C and P availability but not N

Declaration of interests

☐ The authors declare that they have no known competing financial interests or personal relationships that could have appeared to influence the work reported in this paper.

☒ The authors declare the following financial interests/personal relationships which may be considered as potential competing interests:

Davey Jones reports financial support was provided by Biotechnology and Biological Sciences Research Council. Roland Bol reports financial support was provided by German Research Foundation. Barbara Fuentes reports financial support was provided by National Agency for Research and Development. Francisco Remonsellez reports financial support was provided by National Agency for Research and Development. Davey Jones reports financial support was provided by Natural Environment Research Council.